Support for global climate reorganization during the "Medieval Climate Anomaly"

N. E. Graham · C. M. Ammann · D. Fleitmann ·
K. M. Cobb · J. Luterbacher

Abstract Widely distributed proxy records indicate that the Medieval Climate Anomaly (MCA; ~900–1350 AD) was characterized by coherent shifts in large-scale Northern Hemisphere atmospheric circulation patterns. Although cooler sea surface temperatures in the central and eastern equatorial Pacific can explain some aspects of medieval circulation changes, they are not sufficient to account for other notable features, including widespread aridity through the Eurasian sub-tropics, stronger winter westerlies across the North Atlantic and Western Europe, and shifts in monsoon rainfall patterns across Africa and South Asia. We present results from a full-physics coupled climate model showing that a slight warming of the tropical Indian and western Pacific Oceans relative to the other tropical ocean basins can induce a broad range of the medieval circulation and climate changes indicated by proxy data, including many of those not explained by a cooler tropical Pacific alone. Important aspects of the results resemble those from previous simulations examining the climatic response to the rapid Indian Ocean warming during the late twentieth century, and to results from climate warming simulations—especially in indicating an expansion of the Northern Hemisphere Hadley circulation. Notably, the pattern of tropical Indo-Pacific sea surface temperature (SST) change responsible for producing the proxy-model similarity in our results agrees well with MCA-LIA SST differences obtained in a recent proxy-based climate field reconstruction. Though much remains unclear, our results indicate that the MCA was characterized by an enhanced zonal Indo-Pacific SST gradient with resulting changes in Northern Hemisphere tropical and extra-tropical circulation patterns and hydroclimate regimes, linkages that may explain the coherent regional climate shifts indicated by proxy records from across the planet. The findings provide new perspectives on the nature and possible causes of the MCA—a remarkable, yet incompletely understood episode of Late Holocene climatic change.

Keywords Medieval Climate Anomaly · Little Ice Age · Tropical SSTs · Global climate dynamics

N. E. Graham (✉)
Hydrologic Research Center, San Diego, CA, USA
e-mail: ngraham@hrc-lab.org

N. E. Graham
Scripps Institution of Oceanography, La Jolla, CA, USA

C. M. Ammann
National Center for Atmospheric Research, Boulder, CO, USA

D. Fleitmann
Institute of Geological Sciences, University of Bern,
Bern, Switzerland

D. Fleitmann
Oeschger Centre for Climatic Change Research,
University of Bern, Bern, Switzerland

K. M. Cobb
Georgia Institute of Technology, Atlanta, GA, USA

J. Luterbacher
Justus-Liebig-University, Giessen, Germany

1 Introduction

It has long been observed from proxy data that global climate during the past 1200 years can be divided into two periods, the "Medieval Climate Anomaly" (MCA, about 900–1350 AD) and the subsequent "Little Ice Age" (LIA; about 1500–1850) (e.g. Lamb 1965; Grove 1988). An early regional synthesis of MCA climate was provided by

H. H. Lamb, who used documentary records to outline the case for general warmth in the North Atlantic-European sector and increased cool season precipitation across Britain during medieval time (Lamb 1965). Lamb, a meteorologist, recognized that the available evidence implied a "…shift in the upper westerlies, the depression tracks should have had an average position 1–3° north of the modern normal (1900–1939) position—a displacement that probably implies less sea ice …"—(Lamb 1965; also Lamb 1969), thus emphasizing the relationship between changes in circulation and surface climate, and the idea of modest (comparable with modern interannual variability) but persistent shifts in winter circulation over the North Atlantic and Europe during the MCA.

LaMarche (1974) used multi-elevation tree-ring and other data to infer late Holocene climate changes in the White Mountains of California. His analyses indicated that conditions were predominantly warmer and drier from ∼1000–1300 AD and cooler, wetter from ∼1400–1800 AD, and showed that such changes could be explained by a northward-to-southward shift of the storm track over the region. LaMarche pointed out that the MCA-LIA changes over the western US were synchronous with those inferred by Lamb (1965) for the North Atlantic and Western Europe, possibly indicating a shift in global circulation patterns, much as surmised by Lamb (1969).

Succeeding decades have seen the development of much further evidence concerning MCA-LIA climate from the Atlantic-European and North America sectors, and at widely distributed sites around the world. While many of these records show indications of notable climate shifts associated with the MCA, it became apparent that this period was characterized not by uniformly warmer temperatures, but rather by a range of temperature, hydroclimate and marine changes with distinct regional and seasonal expressions (Folland et al. 1992; Hughes and Diaz 1994; Bradley 2000; Bradley et al. 2003). The general idea of a tendency for stronger cool-season North Atlantic westerlies during the MCA, as occurs with a more positive North Atlantic Oscillation (NAO), has persisted and been discussed as a possible driver to explain changes in diverse regional proxy records (e.g., Keigwin 1996; Proctor et al. 2000; Mangini et al. 2005; Lund et al. 2006; Esper et al. 2007; Sicre et al. 2008a; Massé et al. 2008; Wanamaker et al. 2008; Trouet et al. 2009). Similarly, evidence for cool-season aridity and related climate changes in the western US during medieval times is now available from a wide range of proxy and archeological records (e.g., Muhs 1985; Mehringer and Wigand 1990; Swetnam 1993; Stine 1994; Hughes and Funkhouser 1998; Kennett and Kennett 2000; Cook et al. 2004; Jones and Schwaitalla 2008; see Woodhouse 2004; Graham et al. 2007 for reviews), indicating a northward shift in the boreal winter storm track

across the eastern North Pacific and western North America and a contraction and/or westward shift in the Aleutian Low (Stine 1994; MacDonald and Case 2005; Graham et al. 2007; Seager et al. 2007a, 2008).

The idea of coherent large-scale changes in circulation over the North Pacific received additional attention with the development of evidence from fossil coral records, as well as marine and lacustrine sediments which consistently point to cooler sea surface temperatures (SSTs) and significantly drier conditions in the central and eastern equatorial Pacific during the MCA (Cobb et al. 2003; Rein et al. 2004; Conroy et al. 2008b). Given the well established associations between winter North Pacific circulation patterns, cool season precipitation over the western US, and interannual-to-interdecadal SST variability in the tropical Pacific (Bjerknes 1969; Lau 1985; Schonher and Nicholson 1989; Mantua et al. 1997; Rajagopalan et al. 2000), the proxy evidence is consistent with the idea that MCA aridity in the American West (and contraction of the Aleutian Low) was a response, at least in part, to cooler central and eastern tropical Pacific SSTs. This idea has been explored by consideration of available proxy data and model results (Graham et al. 2007; Seager et al. 2007a, 2008). One important result from some of these latter studies has been the suggestion that while many of these MCA-LIA climate anomalies can be explained by changes in tropical Pacific SSTs alone, others suggest an important role for SST changes elsewhere.

Proxy evidence relating to MCA-LIA climate changes from other regions around the planet has become more plentiful over recent decades as well. While these records are diverse with respect to interpretation, calibration, sensitivity and resolution, it is now possible to use the more complete proxy network presently in place to attempt qualitative interpretations of linked climate/circulation changes at larger spatial (hemispheric) scales. Some of these more recently available records show distinctive MCA-LIA changes in North Atlantic SSTs and sea ice (Sicre et al. 2008a; Massé et al. 2008), Meso-American/Caribbean/Gulf of Mexico climate and oceanic conditions (Haug et al. 2003; Lund et al. 2006; Richey et al. 2007), tropical African rainfall (Verschuren 2004; Verschuren et al. 2000; Russel et al. 2007; Shanahan et al. 2009), and the Indian and East Asian monsoons (von Rad et al. 1999; Sinha et al. 2007; Zhang et al. 2008).

A principal hypothesis supported by our results, and suggested by a recent reconstruction of MCA-LIA temperature contrasts (Mann et al. 2009), is that MCA-LIA climate change involved opposing changes in Indo-Pacific warm pool and central/eastern tropical Pacific SSTs (i.e., changes in the tropical Indo-Pacific zonal SST gradient), with the resulting circulation changes driving a variety of surface climate shifts around the planet. We explore this idea using

a synthesis of globally distributed proxy records and results from new coupled model experiments examining the response to a warmer Indian-West Pacific Ocean. The model results are also discussed in the context of previous experiments bearing on the role of tropical SSTs in driving recent and past climate change (e.g., Rodwell et al. 1999; Branstator 2000; Hoerling et al. 2001; Bader and Latif 2003; Giannini et al. 2003; Hurrell et al. 2004; Hoerling et al. 2004; Deser and Phillips 2006; Graham et al. 2007; Seager et al. 2008), and others examining the climate response to changes in irradiance and high latitude temperatures (e.g., Clement et al. 1996; Shindell et al. 2001; Meehl et al. 2003; Sun et al. 2004; Mann et al. 2005; Pierce et al. 2006; Ammann et al. 2007; Timmermann et al. 2007a, b, Lu et al. 2007).

In the presentation that follows, Sect. 2 describes the data, methods and models. Section 3 presents a new circulation and hydroclimatic summary of indications for MCA climate based on proxy records and regional reconstructions, and the results from the coupled model experiments and those from similar experiments. Section 4 provides a discussion synthesizing the proxy data and coupled model results and possible forcing mechanisms for the tropical SST changes inferred for the MCA. Section 5 provides a brief summary.

2 Methods and data

2.1 Coupled model experiments

2.1.1 Tropical warming simulations

Coupled global climate model (CGCM) simulations (collectively the "IOWP simulations") were performed with various configurations of warming prescribed over tropical Indian and western Pacific oceans (IOWP) SSTs. The experimental design was motivated by proxy evidence for medieval climate changes not well explained by a cooler tropical Pacific alone (as discussed above) and model simulations showing that warmer Indian Ocean SSTs produce important features of inferred MCA climate changes (e.g., Bader and Latif 2003; Hurrell et al. 2004; Hoerling et al. 2004). We used the National Center for Atmospheric Sciences (NCAR) Community Climate System Model (CCSM, v. 3.0.1 beta 14; Collins et al. 2006; Kiehl et al. 2006) with the atmospheric model configured at triangular-31 spectral truncation (about 3.75° resolution) and 26 vertical levels, and the ocean model with 40 vertical levels, zonal resolution of 1.8°, and meridional resolution varying from 1.8° at higher latitudes to 0.8° in the tropics (Gent et al. 2006). The sea ice model includes both dynamical and thermodynamical treatment (DeWeaver and Bitz 2006; Holland et al. 2006a), and the land surface is simulated

with improved hydrology (Bonan and Levis 2006; Dickinson et al. 2006). The different component models communicate through a flux coupler (Collins et al. 2006). This version of CCSM has a generally realistic climatology, though El Niño-Southern Oscillation (ENSO) variability is highly periodic with a 2-year period, the Pacific equatorial cold tongue penetrates too far to the west, and a double ITCZ is present in the tropical Pacific (Hurrell et al. 2006; Neale et al. 2008; a problem shared by many coupled models, Guilyardi et al. 2009; Bellucci et al. 2010). The model qualitatively reproduces cool-season ENSO teleconnections over the North Pacific and North America, but the response pattern over the eastern North Pacific and western US is displaced well to the north of the observed position, and shows an unrealistic feature over the southwestern US and northern Mexico (see Sect. 3.2).

In our experiments, IOWP temperatures were warmed by prescribing increased surface shortwave flux into the ocean. The results described in the text come from a simulation using 25 W m^{-2} additional shortwave flux from 15°S–25°N latitude and 40–160°E (the "IOWP25" simulation). Two other simulations used 10 and 15 W m^{-2} of additional flux over the same region ("IOWP10" and "IOWP15", respectively), and another simulation ("IO10") used with 10 W m^{-2} forcing over the restricted to west of 100°E. The regions where additional irradiance was prescribed are shown in Fig. 1 and details of the experiments are given in Table 1. Regional and global temperatures rise in the IOWP warming experiments in response to the additional surface flux—Table 2 gives these changes in SST (global and tropical Indian Ocean) and near-surface air temperature (global and global land-only). Note that the regionally prescribed increase in irradiance is used only to induce warming in the tropical Indian-Western Pacific Oceans and is not proposed as a mechanism for any actual changes.

ENSO behavior changed very little in the tropical warming experiments, tending towards a slightly less periodic and higher amplitude cycle (not shown). The simulation results do not show clear tendencies in the Atlantic Meridional Overturning Circulation (AMOC; not shown) with Indian Ocean warming and resulting strengthened NAO (see Sect. 3.2.1), behavior that contrasts with model results reported by Delworth and Greatbatch (2000) and Bader (2005). The former found that NAO-related surface fluxes over the North Atlantic resulted in an enhanced AMOC with a stronger NAO. The latter, using a different model, also found the AMOC closely tracked low frequency changes in the NAO (and Indian Ocean temperatures, which drove the simulated NAO variability), but in this case the AMOC changes resulted from changes in tropical ocean salinity rather than higher latitude surface fluxes.

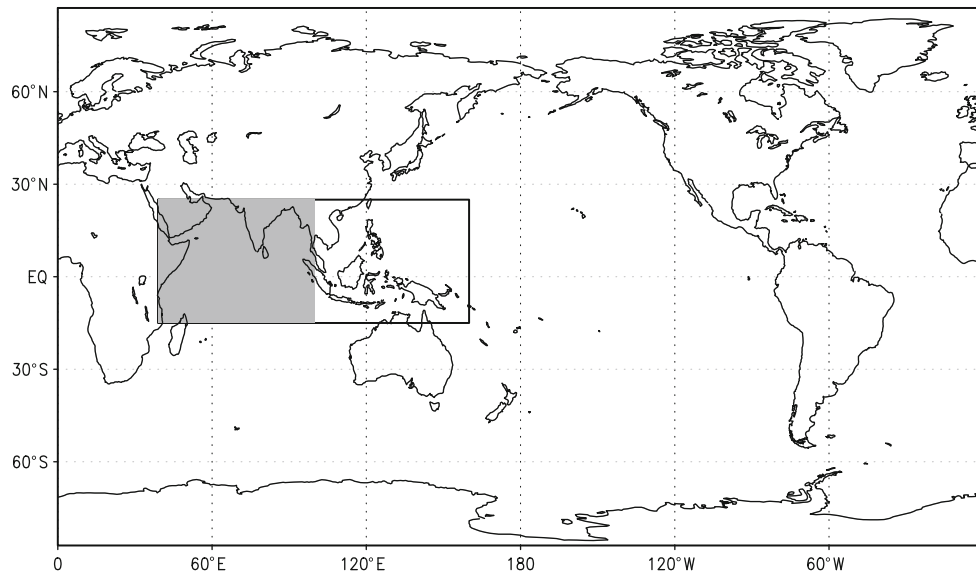All simulations used the same initial conditions and branched from an existing pre-industrial control simulation

Fig. 1 Regions where additional surface irradiance (over the ocean only) was used to increase SSTs in the tropical warming experiments. Full region was used for the IOWP25, IOWP15 and IOWP10 experiments; *shaded area* was used for the IO10 experiment

Table 1 Prescribed (over oceans only) irradiance for tropical warming experiments

Simulation	Region with added shortwave forcing	Additional irradiance (W m^{-2})
IO10	25°N–15°S; 40°E–100°E	10
IOWP10	25°N–15°S; 40°E–160°E	10
IOWP15	25°N–15°S; 40°E–160°E	15
IOWP25	25°N–15°S; 40°E–160°E	25

Table 2 Average SST differences (simulation less CNTL; °C)—global ("SST-GLB"), Indian Ocean average ("SST-IND"; region from the African coast to 100°E and 10°S to 10°N), and average near-surface air temperature over land ("TA-LAND"), and entire globe ("TA-GLB")

Simulation	SST-GLB (SST-IND)		TA-GLB (TA-LAND)	
	DJFM	JJAS	DJFM	JJAS
IO10	0.07 (0.32)	0.07 (0.24)	0.10 (0.15)	0.07 (0.06)
IOWP10	0.15 (0.30)	0.17 (0.36)	0.21 (0.27)	0.21 (0.25)
IOWP15	0.27 (0.52)	0. 28 (0.50)	0.38 (0.53)	0.34 (0.42)
IOWP25	0.45 (0.85)	0.44 (0.89)	0.56 (0.71)	0.55 (0.66)

("CNTL"); each was run out for 48-years. Beyond the prescribed added surface shortwave flux, no other changes in irradiance (e.g., from solar, volcanic or greenhouse gases) were used. Simulated Indian Ocean and western Pacific SSTs appear approximately equilibrated after about 7 years, so most results are expressed as comparisons between years 8 and 48 for the tropical warming simulation results (41 years), and years 1–50 for the CNTL results, counting from the branch point of the former. Comparisons are in the form of differences for temperature (2-m air temperature over land, surface temperature over water) and sea level pressure (SLP) and ratios for precipitation; temperature differences from the CNTL simulation are additionally adjusted for the changes in global average temperature (2-m or surface) resulting from the additional flux climate system. Significance levels are assessed using a *t* test value of 2.0, approximately the 95% confidence level for comparing samples of 41 and 50 [df = 89 $(n_1 + n_2 - 2)$, Sokal and Rohlf 1969]. The tropical warming simulations produce qualitatively similar results and differences with the CNTL climatology tend to scale with the irradiance forcing (and resulting SST anomalies) with some further dependence on the forcing region (see Sect. 3.2)

2.1.2 1150-year late Holocene simulation

We also use results from an 1150-year simulation (Ammann et al. 2007) performed with NCAR CCSM version 1.4 (Boville and Gent 1998) using the same ocean and atmosphere resolution as the tropical warming experiments described above. The model was forced with estimated changes in solar irradiance, greenhouse gas concentrations, and volcanic aerosols from 850 to 1999 AD (see Ammann et al. 2007 for further details), whereas no orbital changes in irradiance were used. This version of CCSM has short-comings with respect to ENSO variability (Meehl and Arblaster 1998) and eastern Pacific/North American tele-connections like those described earlier for CCSM version

3.0.1. The results show good agreement with Northern Hemisphere (NH) temperature reconstructions over the past millennium (Ammann et al. 2007; Jansen et al. 2007), though MCA-LIA changes in large-scale extratropical NH atmospheric circulation, and in differences between warm pool and eastern tropical Pacific SSTs, do not agree with those inferred from proxy records (not shown; see Mann et al. 2009 for further discussion). This simulation had noticeable drift (cooling) through the first few centuries that was removed (using splines for the results shown in Ammann et al. 2007). The results shown in this paper are for North Atlantic "sea ice coverage" for the North Atlantic Ocean over the region 50–25°W and 45–55°N (see Fig. 5C) and come from the original (non-drift corrected) model results, but focus on the latter half of the simulation. Ice cover was estimated from 10-m air temperature assuming sea ice cover if the air temperature <272°K).

2.2 Proxy records

Details and references for many of the proxy records utilized in our study are given in Table 3, and several others are introduced in the text. Figure 2 shows the location and sense of MCA climate change of many of the records. We have emphasized the use of records that are understood qualitatively (or quantitatively) as climatic indicators, have temporal resolution and age model uncertainty less than about 50 years, share patterns of low frequency variability recognizable from observations or model results, and provide insight into dynamics, and large-scale circulation and hydroclimatic patterns. Few, if any, large collections of proxies portray internally consistent scenarios for large-scale MCA climate that differ significantly from those suggested in Sect. 3.1, though there are certainly differences at regional scales where interpretations are dependent on relatively few records. Of the records we have not used, some are open to alternative interpretation (and a few are discussed in the text), or do not bear strongly on the questions at hand by virtue of resolution, dating uncertainty, seasonality, location, or type. Inevitably, some proxy records have not been considered because they were unknown to us or unavailable.

3 Results

3.1 Indications for MCA-LIA climate patterns from proxy records

To provide context for later discussions, this section presents an overview of some large-scale hydroclimate and circulation changes suggested by proxy records over the past ∼1500 years. As most elements of the climatic patterns described have been discussed previously by others (e.g., Lamb 1965; Shindell et al. 2001; Cook et al. 2004; Verschuren et al. 2000, Verschuren 2004; Graham et al. 2007; Seager et al. 2007a, b; Sinha et al. 2007; Trouet et al. 2009; Zhang et al. 2008; Yang et al. 2009), the goal of this section is to portray these elements together in order to highlight and relate regionally coherent climate changes supported by proxy records. The locations of many of the proxy data described are shown in Fig. 2 with time series shown in Figs. 3, 4, 5 and Table 3 providing additional details.

Two of the most fundamental circulation elements that have been proposed for extra-tropical NH winter during the MCA include (i) higher sea level pressure (SLP) in the eastern North Pacific (a contracted Aleutian Low), and (ii) enhanced westerlies across the North Atlantic with a more positive NAO-like circulation pattern (Fig. 2). Evidence for more anticyclonic circulation over the eastern North Pacific is supported by plentiful proxy data indicating reduced MCA precipitation in the western US. This evidence has been reviewed previously (e.g., Woodhouse 2004) and is discussed only briefly in this section. The idea for a stronger NAO-like circulation pattern during the MCA is suggested by terrestrial proxy records from Europe and northwest Africa and marine proxy records from the North Atlantic. For the terrestrial proxies, this idea rests largely on indications for increased precipitation in Britain and drier conditions in northern Morocco (Fig. 3 D, E, H; Lamb 1965; Proctor et al. 2000; Charman et al. 2006; Esper et al. 2007), and for warmer MCA winter temperatures (or fewer harsh winters) in central and northwest Europe (Fig. 3G; Lamb 1965; Pfister et al. 1998; Mangini et al. 2005), all changes consistent with low frequency winter NAO-related variability in the instrumental record (e.g., Hurrell 1995; see discussion in Trouet et al. 2009).

Marine records from the North Atlantic provide some additional support for the idea of a more positive NAO-like circulation pattern during the MCA. Among these are SST reconstructions from near Bermuda (Keigwin 1996; Fig. 3A) and the Gulf of Maine (Wanamaker et al. 2008) indicating MCA SSTs were 1–1.5°C warmer than during the LIA. As noted by Keigwin (1996) and others, warming in this region is consistent with modern NAO-SST relationships (see also Visbeck et al. 2003). From higher latitudes of the North Atlantic, a recent high-resolution reconstruction from the North Iceland shelf (Sicre et al. 2008a) shows a distinctive period of persistently warmer summer SSTs during the MCA bounded by rapid SST changes (∼1°C in 1–2 decades; Fig. 3B; see also Fig. 5D and related discussion). A lower resolution reconstruction developed from a nearby core (Jiang et al. 2005) indicates a similar magnitude of cooling during the transition from the MCA into the LIA. As discussed by Sicre et al. (2008a), the

Table 3 Additional information for proxy records; numbers in first column refer to locations in Fig. 2; letters in parentheses refer to time series in Fig. 3

Indices and location	Climate indicator	Type	References
1(A). Bermuda/Sargasso Sea	Annual SST	Marine sediment core, foraminifera δ^{18}O	Keigwin (1996)
2. Gulf of Maine, northeast USA	Annual SST	Bivalve δ^{18}O	Wanamaker et al. (2008)
3(B). North Iceland	Summer SST	Marine core, algae alkenone	Sicre et al. (2008a)
4(C). North Iceland	Winter sea ice	Marine core, sea ice biomarker	Massé et al. (2008)
5. Southwest Greenland	Winter sea ice	Marine core, diatom index	Jensen et al. (2004)
6(D). Scotland	Cool season precipitation	Speleothem varve width	Proctor et al. (2000); also, Charman et al. (2006)
7(E). England-Wales	Sept.–June precipitation	Documentary	Lamb (1965)
8. Western Europe	Winter temperature	Documentary	Pfister et al. (1998)
9(F). Alps regional average	Winter temperature	Historical, instrumental	Luterbacher et al. (2004)
10(G). Austrian Alps (Spannagel)	Winter temperature	Speleothem δ^{18}O	Mangini et al. (2005); data in Fig. 2 as calibrated in Trouet et al. (2009)
11. Swiss Alps	Summer temperature	Tree-rings width	Büntgen et al. (2006)
12(H). Morocco	Winter precipitation	Tree-ring width	Esper et al. (2007)
13(I). Kenya, Uganda	Lake level, precipitation	Lake sediment cores, various	Verschuren et al. (2000, 2004), Russel et al. (2007)
14(J). Main Nile—Cairo, Egypt	Nile flood level—Ethiopian Highlands (summer precipitation)	Historical-documentary (measured)	Hassan (1981); also Kondrashov et al. (2005), Hassan (2007); data in Fig. 2 from D. Kondrashov
15. Ghana	Lake level, summer precipitation	Lake sediment core, various	Shanahan et al. (2009)
16(L). Southern Oman	Summer precipitation	Speleothem δ^{18}O	Fleitmann et al. (2003)
17(K). Northern Oman	Winter precipitation	Speleothem δ^{18}O	D. Fleitmann, unpublished record from northern Oman
18(M). Guliya Ice Cap, northwestern Tibetan Plateau	Winter precipitation	Ice core, snow accumulation rate,	Thompson et al. (1995), Yang et al. (2009); see also Wang et al. (2007), data shown in Fig. 2 contributed by L. Thompson
19. Coastal Oman	Summer upwelling	Marine core, foraminifera abundance	Anderson et al. (2002)
20. Coastal Pakistan	Summer precipitation	Marine sediment core	von Rad et al. (1999); also Agnihotri et al. (2002), Agnihotri and Dutta (2003)
21. Eastern Indian Peninsula	Summer precipitation	Speleothem δ^{18}O	Sinha et al. (2007)
22. Coastal southern China	Summer precipitation	Speleothem δ^{18}O	Wang et al. (2005)
23. Central China	Summer precipitation	Speleothem δ^{18}O, documentary	Zhang et al. (2008); also Tan et al. (2008)
24. Southeastern China	Summer precipitation	Documentary	Zheng et al. (2006)
25(N). Indonesia—Makassar Strait	Western tropical Pacific SST	Marine sediment core, foraminifera δ'^{18}O	Newton et al. (2006); also Oppo et al. (2009)
26(O). Palmyra	SST (central equatorial Pacific)	Coral δ'^{18}O	Cobb et al. (2003)
27(P). Galapagos Islands, eastern equatorial Pacific	SST (eastern equatorial Pacific)	Lake sediment core, diatom index.	Conroy et al. (2008b)
28(Q). Coastal Peru	High river flow, N. Peru	Marine core riverine sediment	Rein et al. (2004)
(R) Central Chile	High inflow, flooding	Lake core, flood deposits	Jenny et al. (2002)
29. Panama	Wet season (June–September) precipitation	Speleothem δ'^{18}O	Lachniet et al. (2004)
30. Yucatan	May–October precipitation-evaporation	Lake core, various indices	Hoddell et al. (1995)

Table 3 continued

Indices and location	Climate indicator	Type	References
31(S). Western USA	Cool half-year precipitation, warm season soil moisture	Tree-ring width	Cook et al. (2004), also Mehringer and Wigand (1990); Stine (1994), Hughes and Funkhouser (1998); see Woodhouse (2004), Cook et al. (2004), and Graham et al. (2007) for reviews
32. Coastal Venezuela	Warm season precipitation	Marine core riverine sediment	Haug et al. (2001, 2003)
33. North Atlantic	Winter NAO, strength of mid-latitude westerlies into western Europe.	Various	Lamb (1965), Trouet et al. (2009); also Keigwin (1996), Sicre et al. (2008a), Pfister et al. (1998), Mangini et al. (2005)
34. North Pacific	Winter Aleutian Low	Various	MacDonald and Case (2005), Graham et al. (2007), Seager et al. (2007, 2008)

Fig. 2 Indications from some climate proxy records of how MCA climate differed from that in post-medieval times. *Letter indices* correspond to time series in Fig. 3; numbers correspond to entries in Table 3
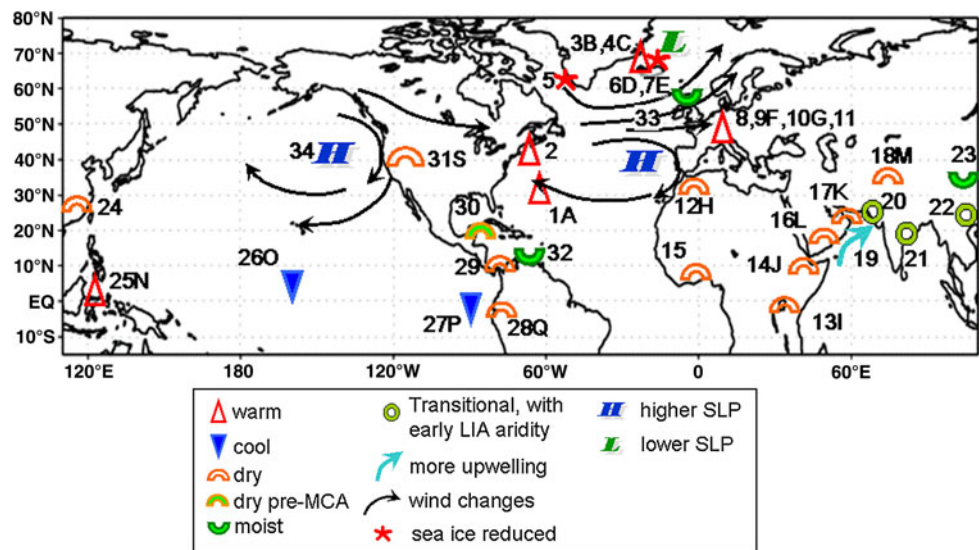
MCA warming on the North Iceland Shelf appears to have resulted from enhanced poleward transport of the warmer waters from the North Atlantic Drift in the North Iceland Irminger Current, possibly due to increased southwesterly winds or to changes in transport associated with the AMOC.

Following the termination of the MCA warming episode seen in the North Iceland SST records, indications of in situ (presumably winter) sea ice appear at the site, becoming more prevalent through the LIA (Massé et al. 2008; Fig. 3C). These indications are consistent with regional documentary records (Ogilvie 1992; Ogilvie and Jónsson 2001; see discussion in Massé et al. 2008), marine proxy evidence for reduced sea ice and increased Irminger Current influence along the coast of southwest Greenland during the MCA (Jensen et al. 2004), and medieval ice cap retreat in the Canadian Arctic (Anderson et al. 2008; see further discussion related to Figs. 5 and 7).

Moving from Europe into Africa and central Asia, a number of other proxy records show temporally coherent features of hydroclimatic change through the past ~1200 years. For summer, documentary measurements of Nile maximum flood level from Cairo (Fig. 3J) indicate maximum annual flood levels tended to be lower during the MCA than during the LIA (Hassan 1981; Kondrashov et al. 2005; Hassan 2007). As described in Appendix 1, converting the maximum flood level record to flood season discharge at Aswan, and applying corrections for channel aggradation, indicates flood season Nile discharge was reduced by about 10% during the MCA. Because more than 90% of Nile flood discharge is comprised of runoff from the Ethiopian Highlands (Sutcliffe and Park 1999), a reduction most likely indicates reduced MCA rainfall in the Highlands, likely reflecting restricted northward migration of the ITCZ during the MCA. This idea is consistent with lacustrine proxy records from Lake Turkana (northwest
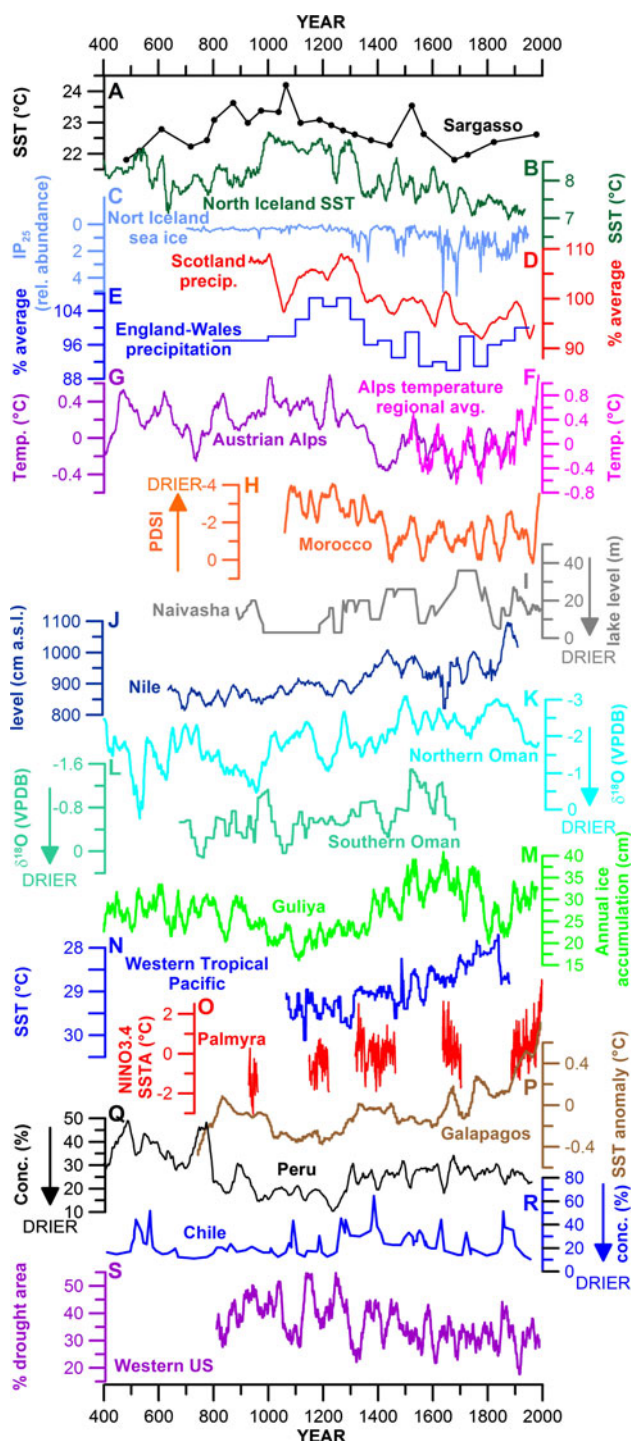
Fig. 3 Some representative late Holocene proxy records. **A** Sargasso Sea annual average SST (marine core). **B** North Iceland summer SST (25-year moving window; marine core). **C** North Iceland winter sea ice (marine core). **D** Scotland cool-season precipitation (speleothem; 51-year moving average). **E** England-Wales Sept.–June precipitation (documentary, 50-year averages). **F** Alps region winter temperature (documentary-historical; 25-year moving average). **G** Alps region winter temperature (speleothem; 25-year moving window; compare with F). **H** Morocco drought index (tree-rings; 25-year moving window). **I** Lake Naivasha (Kenya) level (lake core). **J** Nile maximum flood level, Cairo (historical; 25-year moving average). **K** northern Oman winter precipitation (speleothem, 25-year moving window). **L** southern Oman summer precipitation (speleothem, 25-year moving window). **M** Guliya Ice Cap (northwest Tibetan Plateau) winter precipitation (ice core, 25-year moving average). **N** Tropical Indo-Pacific SST (marine core, 25-year moving window). **O** Central equatorial Pacific SST (fossil coral). **P** Galapagos Islands SST anomaly (lake core). **Q** Peru river discharge (marine core, 25-year moving window). **R** central Chile winter floods (lake core). **S** Western North America drought area (25-year moving average). See Table 3 additional information

tropical Pacific SSTs (Ogallo 1987; Nicholson and Kim 1997), these indications have been noted as consistent with cooler central and eastern tropical Pacific SSTs during the MCA (Cobb et al. 2003; Graham et al. 2007; Seager et al. 2007a). Clear proxy evidence of lower lake level and reduced precipitation during the MCA are also apparent in lacustrine records from Guinea Coast region of tropical West Africa (Ghana; Shanahan et al. 2009; see Fig. 5I and related discussion). Taken with the records from East Africa discussed above, the proxy information suggests reduced rainfall across much of near-equatorial Africa during the MCA.

Other proxy records from the Arabian Peninsula and from central Asia indicate reduced cool-season precipitation extending far eastward from the Mediterranean during the MCA. These include those from the mountains of northern Oman (D. Fleitmann, unpublished record; Fig. 3K) and from a regional reconstruction in central Asia north of the Himalaya (Yang et al. 2009), as suggested by the Guliya ice cap accumulation record (Thompson et al. 1995; Wang et al. 2007; Fig. 3M).

Proceeding through southern Asia, proxy records of monsoon precipitation for coastal Pakistan (von Rad et al. 1999; Agnihotri et al. 2002; Agnihotri and Dutta 2003), western India (see discussion in Sinha et al. 2007), and the southern coast of China (Wang et al. 2005) show a transition towards a pattern in which the driest periods during the last millennium occur early in the LIA—between about 1300 and the late 1500s AD (Fig. 4; see Sinha et al. 2007) This pattern indicating early LIA aridity across much of monsoon Asia is also noted by Buckley et al. (2010; not shown), who present tree-ring evidence for episodes of severe fourteenth to fifteenth century drought in southern Southeast Asia that contributed to the decline of the Khmer

Kenya; Halfman et al. 1994; Verschuren 2004) and from southern Oman (Fleitmann et al. 2003; Fig 3L). At the same time, to the south, Rift Valley lake level reconstructions from central east Africa indicate important reductions in rainfall during the MCA (Verschuren et al. 2000; Verschuren 2004; Fig. 3I; Russel et al. 2007). Because late year rainfall variability in this region (one of the two wet seasons) is positively associated with eastern
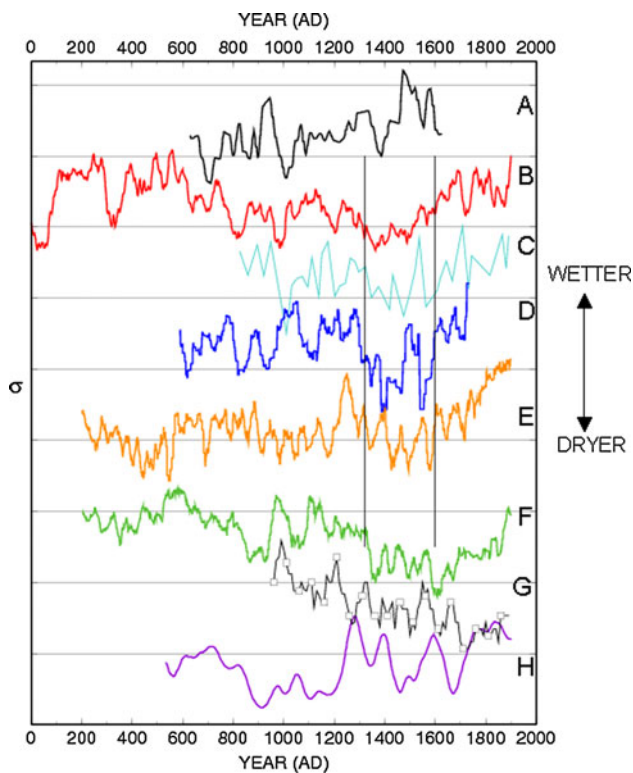
Fig. 4 Proxy time series for the South Asian and East Asian Monsoons. **A** Southern Oman precipitation (Fleitmann et al. 2003; also Fig. 3L). **B** Coastal Pakistan precipitation (von Rad et al. 1999). **C** Coastal Pakistan precipitation (after Agnihotri and Dutta 2003). **D** Central east India precipitation (after Sinha et al. 2007). **E** Coastal southern China precipitation (Wang et al. 2005). **F** Central China precipitation (Zhang et al. 2008). **G** Central China drought-flood index (Tan et al. 2008). **H** Southeastern China precipitation (after Zheng et al. 2006). *Vertical lines* mark early LIA arid period seen in proxy records from coastal Pakistan through southern China (earlier of these lines also marks the rapid MCA-to-LIA cooling in North Iceland SST record (Sicre et al. 2008a; Fig. 3B). All records are Z-scores with offset for display, ordinate gridlines are separated by 3σ

kingdom. Proxy records from central China also show clear evidence for aridity during the LIA, though the timing is shifted roughly a century later than noted above (Figs. 4F,G; Zhang et al. 2008; Tan et al. 2008). Interestingly, documentary records from southeastern China (Zheng et al. 2006) indicate inverse precipitation variability compared to central China (MCA tending to be drier than the LIA in southeastern China; compare Fig. 4E,F with H). Such a pattern of opposing variability in monsoon rainfall over southern and northern China is well documented and characterizes observed and simulated precipitation trends over the latter half of the twentieth century, changes apparently related to shifts in tropical Pacific and Indian Ocean temperatures (see discussions in Li et al. 2008; Zhou et al. 2009).

As noted earlier, the evidence for reduced MCA cool-season precipitation in the western US is widespread and

has been extensively reviewed (e.g., Woodhouse and Overpeck 1998; Woodhouse 2004; Cook et al. 2004; Graham et al. 2007). The general timing of MCA-LIA changes over the West (represented in Fig. 3S by the tree-ring derived drought-area index of Cook et al. 2004) is quite similar to those in Europe, the North Atlantic and the tropical Pacific [e.g., compare Fig. 3S with B, G, H (the shift in the Morocco record is notably later than the others) and P; see also Graham et al. 2007, Seager et al. 2007a], with the most widespread aridity in western US occurring between 900 and 1350 AD. Such a decrease in precipitation over the western US implies a northward shift in the storm track over the region and over the eastern North Pacific during the MCA, with a weaker (or contracted) Aleutian Low and a stronger Northeast Pacific High off the west coast of the US, as indicated by some reconstructions (MacDonald and Case 2005; Graham et al. 2007). A nearly synchronous pattern of MCA aridity transitioning to wetter conditions during the LIA is portrayed by lake sediment records from central Chile (Jenny et al. 2002; Fig. 3R). This inter-hemispheric symmetry of multi-centennial hydroclimatic signals, much as seen in association with modern ENSO variability (Ropelewski and Halpert 1987), is suggestive of a role for tropical Pacific SSTs in driving the similar MCA-LIA hydroclimate differences in these two regions, and for the more general idea that tropical (rather than extratropical) SSTs played a direct causal role in producing extratropical MCA-LIA circulation changes (see Kushnir et al. 2002; Graham et al. 2007).

In Meso-America, archeological evidence and proxy records from Yucatan indicate increasing aridity through much of the first millennium AD culminating with a series of droughts between 700 and 950 AD that apparently contributed to the collapse of Classic Mayan culture (Hoddell et al. 1995; Gill 2000; Fig. 5J). As shown by Haug et al. (2003), individual episodes of pre-MCA drought correlate with periods of reduced river runoff from northern Venezuela suggesting they may have resulted from southward displacements of the ITCZ across the western Caribbean. It is noteworthy that the epoch of severe droughts in Yucatan ended in the late tenth century, contemporaneous with the onset of medieval climate conditions in a number of other records (notably the North Iceland summer SST proxy, see Fig. 5 and related discussion; also Haug et al. 2003), though arid conditions apparently continued in Panama through much of the MCA (Lachniet et al. 2004; until the end of that record in 1310 AD), while the MCA was relatively wet in northern Venezuela (Haug et al. 2001, 2003).

A number of proxy records from the tropical Pacific suggest that the MCA was characterized by an increased zonal temperature gradient with cooler SSTs in the eastern Pacific and warmer SSTs in the extreme western ocean. For
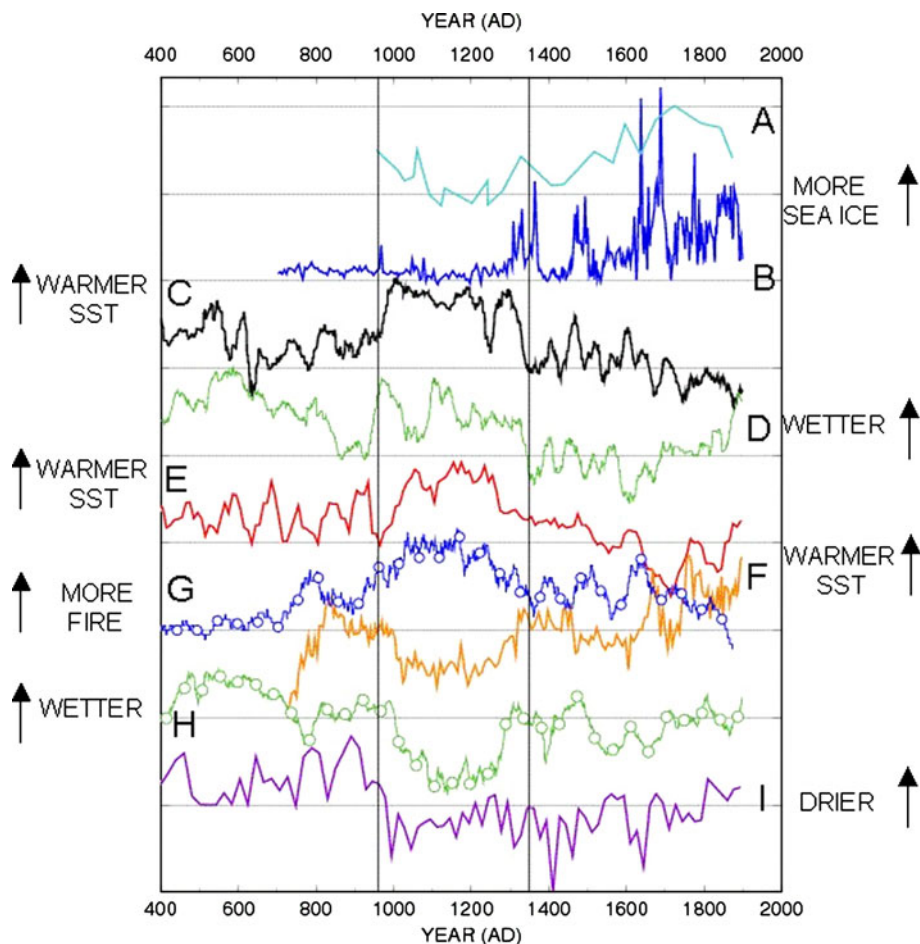
Fig. 5 Contemporaneous high and low latitude changes during the MCA. **A** Southwest Greenland–East Greenland Current/sea ice diatom marker (*light blue*; Jensen et al. 2004). **B** North Iceland winter sea ice from proxy bio-marker (*dark blue*; Massé et al. 2008). **C** North Atlantic sea ice extent (310–335°W, 45–60°N) inferred from near-surface temperature in the 1150-year late Holocene simulation (*red with circles*). **D** North Iceland summer SST anomaly (*black*; Sicre et al. 2008a). **E** Central China monsoon precipitation (*green*; Zhang et al. 2008). **F** Western equatorial Pacific/Indonesian SST anomaly (*red*; Oppo et al. 2009; also Newton et al. 2006). **G** Eastern equatorial Pacific SST anomaly (orange; Conroy et al. 2008b). **H** Sierra Nevada (California) Sequoia grove fire scar frequency (*blue with circles*; Swetnam 1993). **I** Ghana lake silicate concentration index (*green with circles*; Shanahan et al. 2009). **J** Yucatan lake precipitation–evaporation (CaC; Hoddell et al. 1995). All records are Z-scores with offset for display, ordinate grid lines are separated by 3σ. Records B, C, D, E, and I smoothed over 25-year moving windows; record H smoothed with a 51-year running mean; other records show original data

the post-1100 AD period, reconstructed SSTs from the central and eastern equatorial Pacific indicate MCA SSTs averaged ∼0.7–0.8°C cooler than the modern pre-1970 average (Cobb et al. 2003; Conroy et al. 2008b; Fig. 3O, P; Fig. 5G). A marine sediment core from off central Peru (Rein et al. 2004; Fig. 3Q) shows reduced concentrations of riverine sediment during the MCA (suggesting lower precipitation or reduced flood episodes in north coastal Peru) followed by a sharp increase in ∼1250 AD, contemporaneous with increasing reconstructed SSTs in the Galapagos record, and with the timing of the termination of the most arid conditions in the western US and central Chile (compare, Fig. 3O–S).

Sea surface temperature reconstructions from the far western tropical Pacific in Indonesian waters show SST

tendencies strikingly opposite to those from those in the central and eastern ocean (Fig. 3N; Newton et al. 2006; also Oppo et al. 2009). These records indicate that SSTs were ∼1°C warmer during the MCA than during the LIA (and ∼0.5°C warmer than the average value during the preceding 500 years), and about the same as modern values. These records also indicate that sea water salinity has tended to vary in phase with SST over the last millennium, so ocean surface conditions during the MCA were warmer and more saline relative to the LIA. It is plausible that these changes are indicative of a more northerly (southerly) position of ITCZ over the western tropical Pacific during the MCA (LIA) (Newton et al. 2006), and a relatively weaker (stronger) winter monsoon during the MCA (LIA) (Oppo et al. 2009; see also Timmermann et al. 2007a, b).

Whatever the mechanisms governing the MCA-LIA changes in Indonesian SST and salinity, the similarity between these records and others is striking (see Figs. 3, 5) in indicating a shift towards MCA conditions in late tenth century and towards LIA-like conditions between 1250 and 1350 (see further discussion in Sect. 4).

It is important to point out that some regional proxy records appear to be at odds with the idea of cool SSTs in the central-eastern tropical Pacific during medieval time (Graham et al. 2007; Conroy et al. 2008b). These include the records from Laguna Pallcacocha in the equatorial Andes (Moy et al. 2002; high inflow events recorded in sediment), and from Quelccaya Ice Cap in southern Peru (δ^{18}O; Thompson et al. 1984). The Pallcacocha record indicates more high precipitation/high inflow events (interpreted as more El Niño episodes) during the MCA than during the LIA (Moy et al. 2002; see also Conroy et al. 2008a, b). This interpretation may be correct, but if so, it complicates the interpretation of the proxy precipitation records from the western US and Chile, both regions where heavier rainfall during El Niño episodes contributes importantly to the average rainfall association in the instrumental record. The Quelccaya δ^{18}O record shows little change during the MCA and much more depleted values late in the LIA. Interpretations of this record vary (Hoffmann 2003) as to the relative contributions of temperature (Thompson et al. 1984) or precipitation (Vuille et al. 2003a, b) changes in producing the isotopic fluctuations in the Quelccaya record, and whether these relationships have been stable through time, so the regional climatic interpretation of Quelccaya's persistently depleted δ^{18}O during the LIA remains unclear.

3.1.1 Contemporaneous rapid climate changes during the MCA

Although the onset and termination of the MCA are gradual in many proxy records shown in Figs. 3 and 4, in other records these transitions are sharp and coherent. Because such changes raise the possibility of rapid adjustments within the global coupled climate system, some of these records are discussed below, including some considerations related to physical processes, as well as proxy location and sensitivity.

A convenient place to begin this discussion is with the North Iceland summer SST record above (Sect. 3.1; Sicre et al. 2008a; Fig. 3B, also Fig. 5D) with its distinctive decadal-scale transitions in summer SST regimes in the late tenth (warming) and early fourteenth (cooling) centuries. The rapidity of these transitions suggest they may reflect regime-like changes in high latitude North Atlantic sea extent, as supported for Iceland waters at the MCA-LIA transition by the North Iceland ice biomarker record

described earlier (Massé et al. 2008; Figs. 5B, 3C) and documentary records (Ogilvie 1992; Ogilvie and Jónsson 2001; also Massé et al. 2008). That such changes had regional extent is suggested by ice-related marine proxy records from southwest Greenland (Jensen et al. 2004; Fig. 5A), which indicate both a decrease in sea ice at the onset of the MCA and an increase at the termination. Other evidence suggesting the extent of these MCA changes comes from archeological evidence for reduced summer sea ice in the maritime Canadian Arctic (Mudie et al. 2005) and proxy evidence for widespread retreat Baffin Island ice caps during the period $\sim$1000–1250 AD with subsequent rapid expansion going into the LIA (Anderson et al. 2008). Notably, there is little suggestion of a sharply defined medieval event in a collection of trans-arctic proxy temperature records covering the past two millennia (Kaufman et al. 2009), perhaps indicating that temperature fluctuations related to MCA-LIA sea ice changes were largest and may be best recorded in proxies records from regions not far removed from the summer sea ice limit.

Whatever the true spatial extent and character of the MCA transitions on the North Iceland Shelf, it is remarkable that similarly timed abrupt shifts are apparent in proxy records from regions far removed from the North Atlantic. For example, the timing of the North Iceland changes correspond closely to a well-defined increase in rainfall in central China near the northwesterly limit of the East Asian Monsoon (EAM; Zhang et al. 2008; Fig. 5E, also Fig. 4F). As discussed by Zhang et al. (2008), this record shares features in common with a number of indices related to NH temperature, suggesting the possibility that the increased rainfall in this region resulted from greater inland penetration of the EAM during the MCA in response to warmer NH summer temperatures.

Marine proxy records from the far western equatorial Pacific show a similar event-like shift, with a well defined period of warmer SSTs (and higher salinity) during the MCA (Fig. 5F, Oppo et al. 2009; also Fig 3N, Newton et al. 2006). The timing of this episode corresponds well to the period of increased monsoon rainfall in the central China record described above (Fig. 5E; see discussion in Oppo et al. 2009) and to the North Iceland SST excursion. The close agreement between the timing of the North Iceland SST changes and western tropical Pacific SSTs may indicate a dynamical linkage between the changes at these two sites, but if so, it is not apparent whether warmer NH temperatures induced in a northward shift of the winter ITCZ (Newton et al. 2006) and changes in the East Asian Monsoon (see Zhang et al. 2008) and/or a weaker winter monsoon (Oppo et al. 2009), or whether the higher latitude climatic changes were forced from the tropics (Cobb et al. 2003; Graham et al. 2007; Oppo et al. 2009).

Intriguingly, rapid changes opposing those in the western tropical Pacific appear in reconstructed SSTs from the eastern equatorial Pacific (Conroy et al. 2008a, Fig. 5G also Fig. 3P; also in the Peru river runoff reconstruction, Fig. 3Q, Rein et al. 2004) indicating a sharp increase in the zonal tropical Pacific SST gradient going into the MCA. Further evidence of rapid MCA changes coherent with this large-scale signature are seen in a composite fire scar record from the Sierra Nevada in California (Fig. 5H; Swetnam 1993; see also Graham et al. 2007). Notably, the indicated increases in fire frequency are much more constant through the MCA than the regional declines in cool season precipitation (e.g., Fig. 3S, Cook et al. 2004; Graham et al. 2007; Graham and Hughes 2007), suggesting warmer summer temperatures may have contributed further to the sustained elevated fire incidence during the MCA, perhaps as indicated by the simulation results (see Sect. 3.2.2; Fig. 9).

Medieval variability similar to the other records in Fig. 5 is seen in lake level proxy records from Ghana (Lake Bosumtwi; Fig. 5I, Shanahan et al. 2009). The conjunction proxy evidence sharply defined episodes of reduced rainfall in Ghana (and, as noted earlier, simultaneously in eastern equatorial Africa, see Russel et al. 2007) and warmer extratropical North Atlantic SSTs during the MCA is notable (compare Figs. 3A, 5D, I). However, the sense of the relationship indicated by these proxy records (reduced rainfall associated with warmer North Atlantic SSTs) is inconsistent with the positive relationship between these indices suggested by comparison between the Ghana records and a tree-ring based reconstruction of the average extratropical North Atlantic SST (the "AMO", Gray et al. 2004) over the past few hundred years (Shanahan et al. 2009). Eastern equatorial Atlantic SSTs are positively associated with monsoon precipitation in Ghana through the instrumental record [see discussions in Opoku-Ankomah and Cordery 1994; though they do not follow with the late twentieth century SST trends in that region (not shown)]; however, reconstructed Gulf of Guinea SSTs (Weldeab et al. 2007) show no indication of a sharply defined cooling episode during the MCA (not shown). Particularly good agreement is apparent between the Ghana precipitation/lake level reconstruction (Fig. 5I) and reconstructed eastern equatorial Pacific SSTs (Fig. 5G; Conroy et al. 2008b), though the modern relationship between these variables is weak (not shown). Comparison of Ghana lake level proxy records (Shanahan et al. 2009) and the Peru river discharge proxy (Rein et al. Fig. 3Q) indicates a close connection between equatorial eastern Pacific SSTs and Guinea Coast rainfall (as suggested by Figs. 5G, I) through the past 2300 years [not shown; correlations between the Peru discharge and Ghana lake silica records is 0.68 (25-year smoothing) and 0.77 for lake $\delta^{18}O$ (51-year smoothing)].

It is worth noting that regional precipitation gradients are strong, and water balance studies (Turner et al. 1996; Shanahan et al. 2007) demonstrate that declines in lake level like those indicated for Lake Bosumtwi during the MCA could result from modest persistent reductions in average precipitation ($\sim 5\%$, well within the range of modern variability in local rainfall), so medieval changes in regional precipitation may well have been relatively subtle.

Finally, note the temporal coherence between the end of the pre-MCA droughts in Yucatan (Fig. 5J) and rapid summer warming on the North Iceland shelf, suggesting the possibility of northward shift in the ITCZ over Meso-America in synchrony with a reduction in the meridional temperature gradient (Haug et al. 2003); though curiously, there is no indication of the end of MCA shift in the Yucatan record. Other records from the region show a similar pattern of sharp changes or trends near the beginning of the MCA (contemporaneous with the end of the Yucatan droughts) without clear indications at the termination. These include northern Gulf of Mexico SSTs (~ 1–$2°C$ decline at the onset of the MCA; Richey et al. 2007; not shown) and inferred Gulf Stream transport through the Florida Straits (~ 5–10% decline and increasingly salinity from the onset the MCA into the LIA; Lund et al. 2006; not shown). It has been suggested that these changes reflect coupled salinity-transport-climate feedbacks modulating AMOC variability (e.g., Lund et al. 2006; Seager et al. 2007a, b; Sicre et al. 2008a); however, at present the proxy evidence for such an association is quite limited and it is unclear how each of the various elements and processes involved may be linked to each other and to larger-scale MCA-LIA climate changes in general.

These results raise interesting possibilities concerning the causes of coherent rapid regional climate changes during the MCA and LIA. First, the changes in North Iceland summer SST (Fig. 5D; Sicre et al. 2008b) resemble abrupt sea ice variability seen simplified and full physics climate models (e.g., Holland et al. 2006b; Merryfield et al. 2008). These studies show that rapid transitions between perennial sea ice cover and ice-free regimes can result from slight changes in heat flux in circumstances where small changes in melt produce large changes in open water area. For the MCA, the abrupt 1°C SST increase in the North Iceland record at the onset of the MCA occurred in the context of a steady cooling trend (about 2°C) during the 1300 years ending in about 700 AD (e.g., Sicre et al. 2008b; see also Anderson et al. 2008; Kaufman et al. 2009). It is plausible that this cooling increased the sensitivity of regional (non-local) Nordic Sea ice cover, allowing abrupt transitions towards much reduced (increased) ice extent near the onset (termination of the MCA) producing the sharp changes in North Iceland SSTs. Possible

triggers for such transitions include (i) changes in surface irradiance, with relatively high irradiance during the MCA (high solar and low volcanic forcing during the MCA) and sharply lower irradiance (low solar, high volcanic forcing) at the onset of the LIA (Crowley 2000; Hegerl et al. 2006; Ammann et al. 2007; see also Anderson et al. 2008), (ii) changes in oceanic heat transport and surface fluxes related to the varying strength of the southwesterly flow across the high latitude North Atlantic (stronger NAO during the MCA, weaker NAO during the LIA; e.g., Lamb 1965; Trouet et al. 2009), (iii) AMOC variability (oceanic heat transport; Sicre et al. 2008a), and (iv) the long term downward trend in summer SST noted earlier (Sicre et al. 2008b). Such an inverse relation between the NAO and ice extent in the Nordic Sea is apparent the modern record (Deser et al. 2000; Visbeck et al. 2003). The idea that irradiance changes played a role in North Iceland sea ice variability during the LIA is supported by the similarity between the sea ice biomarker record (Fig. 5B; Massé et al. 2008) and North Atlantic sea ice cover inferred from the irradiance-forced millennium climate model simulation (Fig. 5C; Ammann et al. 2007; also Crowley 2000; Hegerl et al. 2006; see Sect. 2.1.2).

A second issue relates to why nearly contemporaneous rapid climate changes appear in proxy records from across the planet. How were these changes communicated? Were the effects of rapid changes in tropical Indo-Pacific SSTs transmitted across the planet via circulation changes [as seen in many model results (e.g., Lau 1985; Graham et al. 1993; Hoerling et al. 2001; Alexander et al. 2002; Bader and Latif 2003), including the tropical warming experiments described in Sect. 3.2]? Or, did the modest changes in high latitude North Atlantic SSTs produce clear and immediate impacts on lower latitude climate? Mechanisms for this latter idea have been explored with climate models in the context of much larger changes North Atlantic SSTs in the context of AMOC collapse (up to 8°C; Timmermann et al. 2007b; see also Sect. 4.1), and while these model results are qualitatively similar with some of the proxy records discussed above, their relevance to much smaller MCA SST changes [about 1°C at North Iceland (Sicre et al. 2008a), 1.5°C at Bermuda (Keigwin 1996)] has not yet been demonstrated. It is also possible that the near-contemporaneous MCA changes in the proxy records in Fig. 5 are not directly related, but rather reflect local sensitivities (proxy and/or climate) to slow changes in background conditions or external forcing. If this is the case, then the MCA shifts are conspicuous, but not necessarily indicative of dynamical teleconnections.

3.2 IOWP Simulation Results

This section presents the results from the IOWP coupled model simulations, focusing on differences between averages from the IOWP25 and CNTL experiments in terms SLP, precipitation and temperature (see Sect. 2.2). The presentation describes results first for boreal winter (December–March), then for boreal summer (June–September). Discussions relating the IOWP25 results to those from our other tropical warming experiments are given in Sect. 3.3, and to related experiments by others in Sect. 3.4. The simulation results are considered within the context of the proxy records in Sect. 4.

3.2.1 Boreal winter

Comparisons of the results from the IOWP25 and CNTL simulations for boreal winter are shown in Fig. 6 (SLP and precipitation) and Fig. 7 (temperature). For SLP, the dominant feature is a belt of higher pressure stretching eastward from the mid-latitude northeast Pacific, across the subtropical Atlantic and Mediterranean, and into central and southwest Asia. Lower SLP covers the high latitude North Atlantic, resulting in a more positive NAO-like pattern (the average Iceland-Portugal SLP difference increases by about 6 hPa in the IOWP25 simulation). Precipitation deficits follow the southern flank of the belt of increased mid-latitude SLP, an area including the western US and Morocco, and mark its eastern terminus over southwest Asia. Increased precipitation covers much of the Nordic Seas and Britain, and extends into parts of northwest Europe, so the simulated precipitation pattern over the Europe and northwest Africa is typical of a stronger NAO (e.g. Hurrell and van Loon 1997). The precipitation signal over central east Africa is mixed, with increased rainfall indicated in some near-coastal regions and decreases over the interior (these features are representative simulated total annual precipitation as well (not shown), though note that the spatial resolution of the model is coarse compared with the scales of the important topographic features in this region).

Increased precipitation covers much of the tropical Indian Ocean and northwestern tropical Pacific (where the SSTs were forced to increase). Interestingly, eastern equatorial Pacific rainfall is reduced by 20–30%. These reductions apparently reflect changes in the Walker Circulation induced directly by the increased IOWP SSTs (increased subsidence over the eastern tropical Pacific in response to increased Indo-Pacific precipitation) and local ocean–atmosphere ("Bjerknes") feedbacks involving joint increases in zonal wind stress (up to 30%; not shown), upwelling and cooler SSTs (as much as −0.5°C; see Fig. 7) in the eastern equatorial Pacific. In the west-central equatorial Pacific (between 150E and 180E) decreased precipitation (and accelerating surface easterlies, not shown) marks the edge of the region where additional irradiance has been applied—the
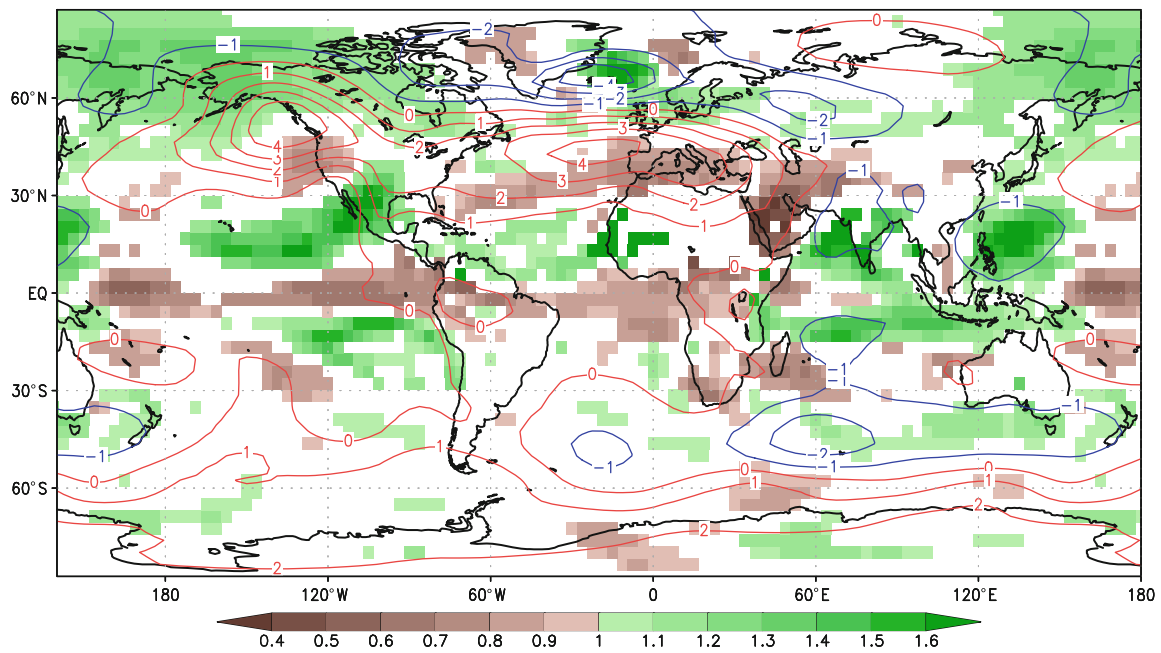
Fig. 6 Differences in December–March precipitation (expressed as fraction of CNTL, color) and SLP (difference, hPa) for the IOWP simulation; precipitation changes are shown only where the differences exceed the 95% confidence level (*t* test) for years 8–48 of the IOWP simulation and 50-years of CNTL data (see Sect. 2.1.1)
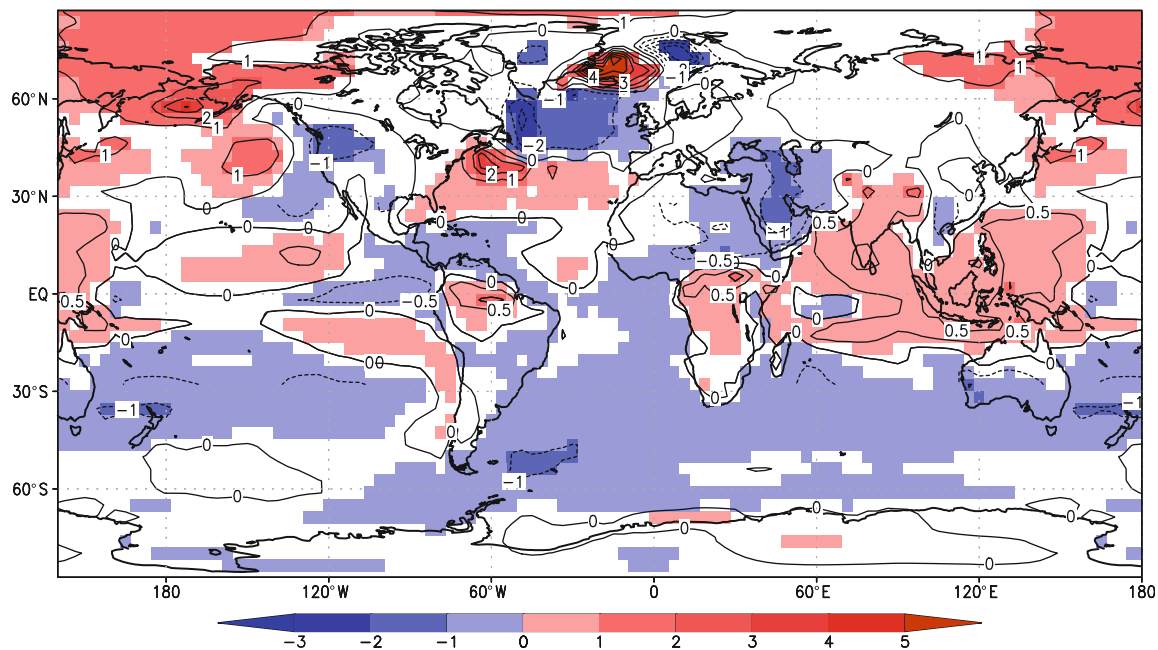

Fig. 7 Differences in December–March temperature between the IOWP25 and CNTL simulations (°C, *color*; values are SST over ocean and 2-m temperature over land). *Colors* are shown only where temperature differences exceed the 95% confidence level (*t* test). Lined contour interval is 0.5°C between 30°N and 30°S and 1°C elsewhere. Global average change in 2-m temperature (SST) has been subtracted from land (ocean) values (see Sect. 2.1.1; Table 2)

prominence of this feature is an artifact of the experimental design.

Simulated changes in winter temperature (Fig. 7) are most conspicuous over the North Atlantic with one band of warmer SSTs extending east from North America between 25°N and 40°N, another band of cooler SSTs reaching across the higher mid-latitudes (40–50°N; beneath the increased surface westerlies), and much warmer
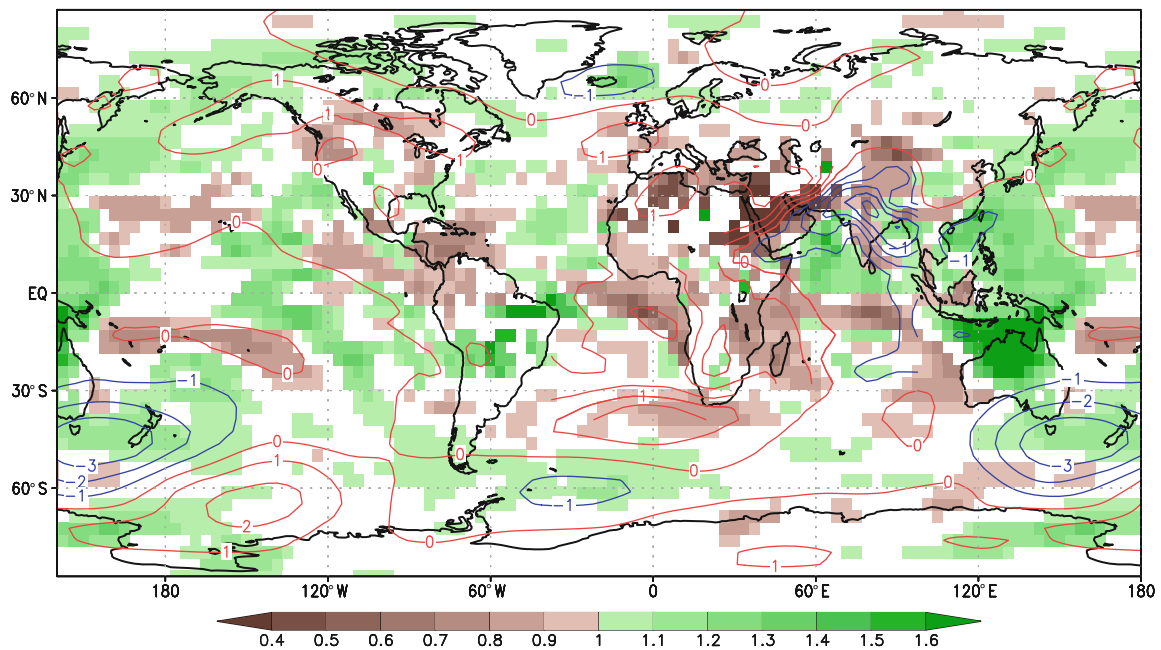
Fig. 8 IOWP25-CNTL differences in summer (June–September) precipitation (expressed as fraction of CNTL, *color*) and SLP (difference, hPa). Precipitation differences are shown only where the differences exceed the 95% confidence level (*t* test; see Sect. 2.1.1). SLP contour interval is 1.0 hPa except 0.25 hPa in the region 30°S–40°N and 25°E–100°E where the finer interval highlights temperature-driven low pressure around continental periphery of northern Indian Ocean (Fig. 6 shows corresponding temperature and surface wind stress changes)

temperatures in the Nordic Seas. Such banded features are typical of the SST response to more positive NAO-like circulation patterns in observations and model data, and arise primarily from atmospheric forcing via changes in surface fluxes of heat and momentum (Cayan 1992; Kushnir 1994; Delworth and Greatbatch 2000; Visbeck et al. 2003). The warming in the Nordic Seas of up to 6°C in winter is associated with a northwestward retreat of the sea ice limit (about 150 km), apparently in response to surface flux and heat transport changes related to a more positive NAO-like circulation pattern and stronger southwesterly winds over the mid-latitude North Atlantic. As noted earlier (Sect. 3.1), such an inverse relationship between NAO-related circulation changes and high latitude North Atlantic sea ice is apparent in the in the instrumental record (Deser et al. 2000; Visbeck et al. 2003), with the sea ice variability resulting from NAO-associated changes in surface heat flux, wind-driven ice transport and increased advection of warmer water from the south.

Elsewhere, the simulated temperature changes show clear warming over the Indo-Pacific region where the irradiance forcing is applied, the induced eastern Pacific cooling noted earlier, and features that generally reflect the sense of changes in advection (inferred from the SLP differences; Fig. 6) over the NH continental regions and surface heat flux over the North Pacific (e.g. Cayan 1992). Consistent with NAO-composites (e.g. Hurrell and van

Loon 1997), the model results do show some warming over northwestern Europe (up to 0.5°C in the Baltic area); these temperature changes do not exceed the *t* test 95% significance limit used for shading (Fig. 7), but are consistent with the regional enhancements in precipitation (Fig. 6; see also Trouet et al. 2009).

3.2.2 Boreal summer

Simulation results for boreal summer are shown in Figs. 8 and 9 (SLP and precipitation, and temperature respectively). For precipitation, the IOWP results show increased rainfall over northern Australia and the Indo-Pacific warm pool, while precipitation deficits cover the continental fringes of the western and northwestern Indian Ocean (see Discussion below), including the Ethiopian Highlands and parts of the southern Arabian Peninsula. Reduced precipitation also covers much of the central and eastern Sahel, but these changes generally do not exceed the 95% *t* test significance level. For the central and eastern Sahel and Ethiopian Highlands the simulated precipitation deficits reflect restricted northward migration of the ITCZ (not shown) during boreal summer, apparently a response to the warmer Indian Ocean SSTs (see further discussion Sects. 3.4 and 4).

The simulation results show reduced precipitation along the Guinea Coast and over the tropical Atlantic Ocean to
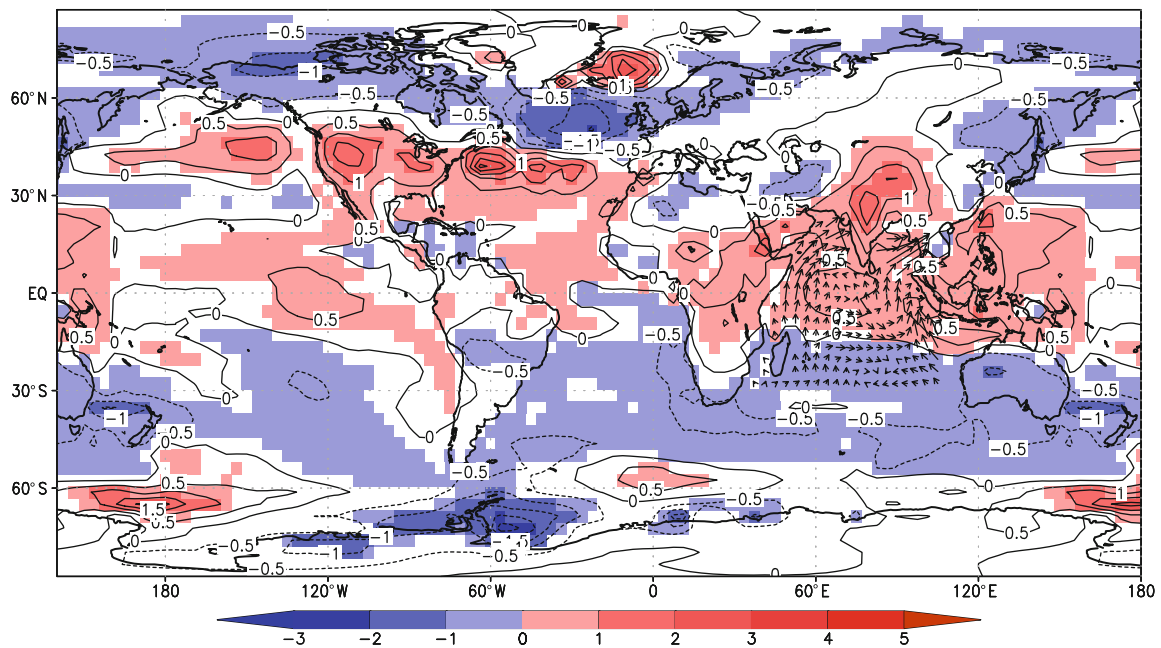
Fig. 9 Differences in June–September temperature (IOWP25-CNTL, *color*; values are SST over ocean and 2-m temperature over land; lined contours at 0.5°C intervals). *Colors* are shown only where the differences exceed the 95% confidence level (*t* test). *Lined contour* interval is 0.5°C. Global average changes in 2-m temperature (SST) have been subtracted from land (ocean; see Sect. 2.1.1; Table 2). *Arrows* show differences in Indian Ocean surface wind stress (τ)

the south. These changes in model precipitation reflect a general decline in rainfall (rather than a meridional shift in the ITCZ). The decrease in regional precipitation is likely indirectly related to presence of relatively cooler simulated SSTs in the eastern equatorial Atlantic (Fig. 9), as seen in observations (e.g. Opoku-Ankomah and Cordery 1994; see also Janicot et al. 1998) and ascribed principally to SST-driven changes in low level humidity (Lamb 1983; Cadet and Nnoli 1987; Vizy and Cook 2002). However, this mechanism does not explain the simulation results because without the adjustment for global average changes (as is done for Figs. 7 and 9, see Sect. 2.1), IOWP25 SSTs in the equatorial Atlantic are slightly warmer than in the CNTL simulation. It is seems most likely that increased large-scale subsidence (presumably from convection over the Indian Ocean) is driving the tropical west African precipitation decline, as well as increased eastern subtropical Atlantic SLP (up to 0.7 hPa; not apparent in Fig. 8) and associated stronger tradewinds (not shown) and cooling in the southeastern tropical and subtropical Atlantic.

The region of reduced rainfall along the continental margins of the northwest Indian Ocean is associated with an elongated "thermal low" centered along the coast (see SLP in Fig. 8). The decreased SLP is evidently a direct thermal response to increased subsidence and higher temperatures over land resulting from the enhanced oceanic convection. The strengthened southwesterly winds (Fig. 9)

along the coasts of northeast Africa and the Arabian Peninsula imply 10–50% increases in wind stress curl and coastal upwelling (not shown), a point touched on further in Sect. 4. The more arid conditions in this region give way to a mixed precipitation signal proceeding east across the Indian subcontinent, and then towards more generally increased precipitation over parts of central and southern China, and southeastern Asia.

The pattern of simulated changes in North Atlantic SSTs during summer are much like those for winter, though with much smaller amplitudes in the Nordic Seas (about 2°C). Warmer temperatures (1–2°C above CNTL values) cover much of the US and southern Canada and extend into the North Pacific, generally following the region of reduced precipitation that traces the southern flank of a ridge of higher SLP along 40–50°N. Cooler temperatures follow the increased westerlies to the north of this anomalous ridge. Widespread reductions in precipitation are depicted across Central America and the southern Caribbean. The summer results show no indications of the cooling and drying over the equatorial Pacific found during the winter months (see Sect. 4.1).

3.3 Results from other IOWP warming experiments

The dominant features of circulation and climate change in the IOWP25 results (Figs. 5, 6, 7, 8) are reproduced in our

other tropical warming simulations and tend to scale with the magnitude and extent of the imposed forcing. Examples of this behavior are shown in Figs. 10, 11, 12, 13, 14, 15, 16, 17, 18 compare results for the different simulations for nine regional indices including the following: (i) the winter NAO, (ii) annual average SST for the western North Atlantic off the US, (iii) winter SST northeast of Iceland, (iv) annual precipitation along the Guinea coast of tropical west Africa, (v) annual precipitation in interior central east Africa (interior coastal region, see below), (vi) summer precipitation in the Ethiopian highlands region, (vii) winter precipitation in central Asia (northwest Tibetan Plateau), (viii) winter precipitation in the eastern equatorial Pacific, and (ix) winter precipitation in the western US.

The repeatability of the simulated winter circulation changes is further demonstrated by pattern correlations (Table 4) between NH δSLP (simulated-CNTL sea level pressure; 30–90°N) from the different tropical warming experiments. These show good agreement between the different simulations, especially between those with warming in both the tropical Indian and western Pacific (IOWP10, IOWP15, IOWP25; pattern correlations ranging from 0.92 to 0.98), which agree less well with simulation with prescribed warming restricted to the Indian Ocean (IO10; pattern correlations 0.63–0.78). The lower NH SLP pattern correlations with the IO10 results primarily reflect differences in the pattern of SLP changes over the North Pacific, with higher SLP dominating all the mid-latitude North Pacific in the IO10 results (not shown), but centered more in the eastern ocean in the IOWP results (as in Fig. 6).

The mid-latitude low pressure anomaly south of Australia and New Zealand in the IOWP25 results for austral winter (Fig. 8) is apparent in the simulations with western Pacific warming, but not in the simulation in which ocean warming was restricted to Indian Ocean (IO10). Similar remarks apply to the increased precipitation over the northwest tropical Pacific (not found in IO10). Interestingly, all of the tropical warming simulations, including IO10, show enhanced precipitation over Australia during austral winter; in terms of total annual precipitation simulated precipitation increases are uniformly largest (20–30%) across southern Australia and result from increases in austral winter precipitation. The heterogeneous pattern of boreal winter precipitation changes over central
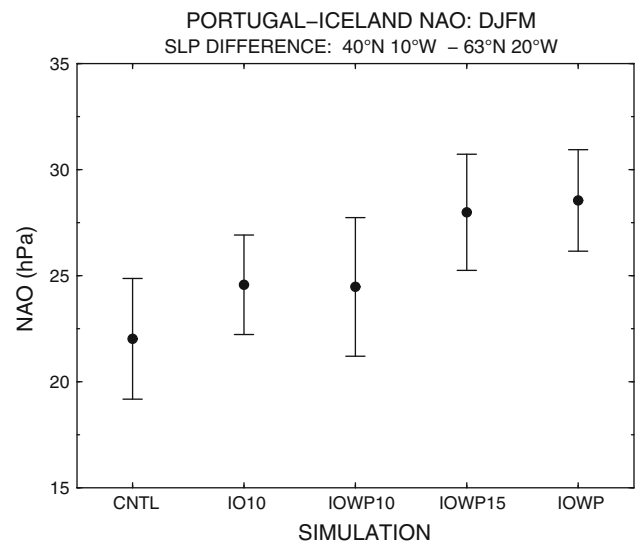

Fig. 10 Portugal-Iceland NAO (difference in SLP between 40°N, 10°W and 63°N, 20°W; hPa) from the different simulations (see Sect. 2.2); average and the 95% confidence range (from t test significance on the means) are shown, these calculated for 50 years from the CNTL simulation and years 8–48 for the tropical warming experiments
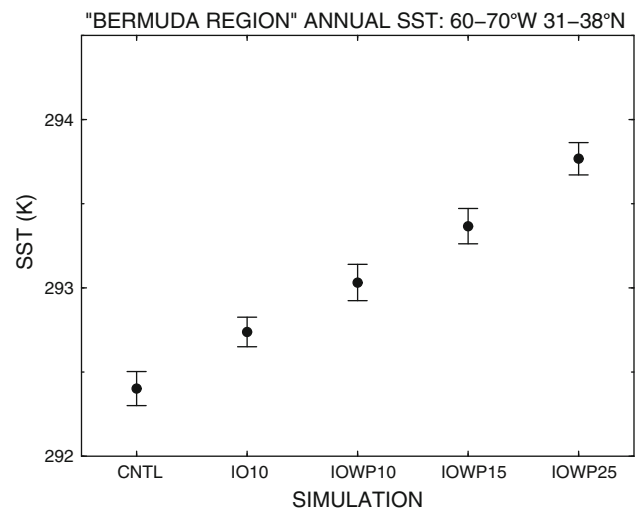

Fig. 11 As in Fig. 10, but for annual average SST (K) from the western North Atlantic (31–38°N, 60–70°W)

East Africa (more rain near the coast, less rain inland) is repeated in our other simulations.

3.4 Relation to other modeling studies using warmer Indian Ocean SSTs

The results from our simulations can be compared to those from other studies examining the climate impacts of altered Indian Ocean and western Pacific SSTs. Most of these fall in two groups; those dealing with the effects on winter
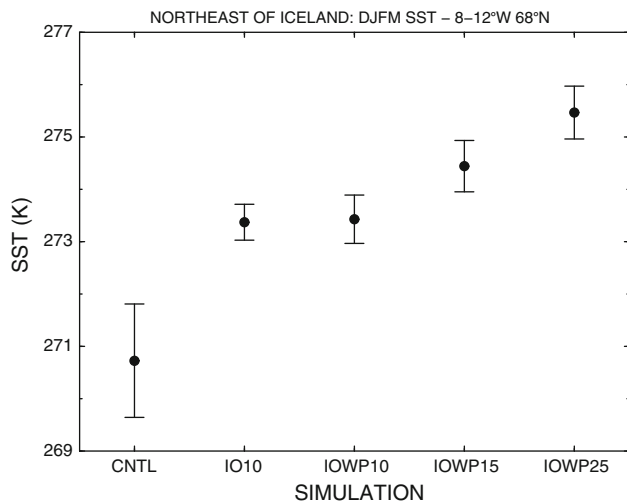
Table 4 Pattern correlations for average winter NH SLP differences (simulated-CNTL; values are for poleward of 30°N, area-weighting was used)

	IOWP10	IOWP15	IO10
IOWP25	0.98	0.96	0.78
IOWP10		0.92	0.78
IOWP15			0.63

Fig. 12 As in Fig. 10, but for December–March SST (K) from northeast of Iceland (68°N, 8–12°W). The larger range in the CNTL simulation SSTs reflects sharp cooling due to sea ice formation in some years; such episodes are absent in the tropical warming simulations. The distributions for summer average SST are similar (not shown), but cover a smaller range (2°C as opposed to 6°C)
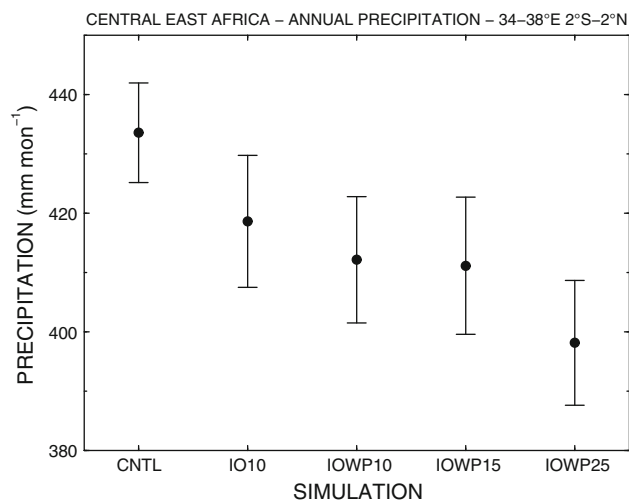

Fig. 14 As in Fig. 10, but for annual precipitation (mm mon⁻¹) from the Ghana, Guinea Coast region tropical West Africa (6°N, 4°W–0°E)
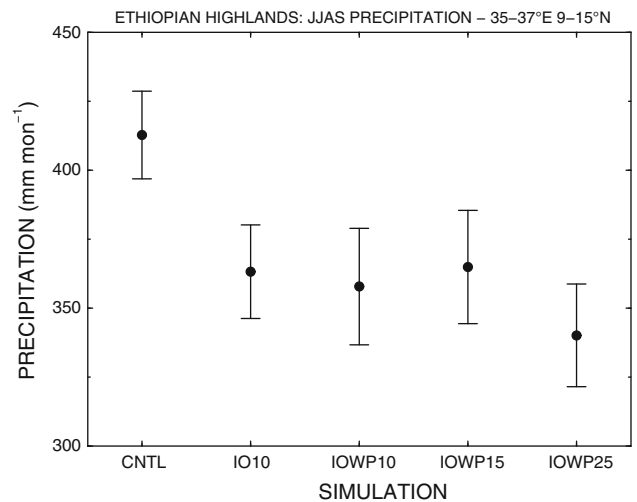

Fig. 13 As in Fig. 10, but for annual precipitation (mm mon⁻¹) from central East Africa (2°S–2°N, 34–38°E)

Fig. 15 As in Fig. 10, but for June–September precipitation (mm mon⁻¹) from the "Ethiopian Highlands" region (9–15°N, 35–37°E)

Northern Hemisphere circulation and the NAO, and those focusing on changes in Sahel precipitation. These studies were motivated largely by the trends towards a stronger NAO (e.g., Hurrell 1995) and reduced Sahel rainfall (e.g., Hulme 1992; Nicholson 2000) during the second half of the twentieth century, and their possible connection to anthropogenic climate change (e.g. Rodwell et al. 1999; Hoerling et al. 2001, 2004, 2006; Giannini et al. 2003; Hurrell et al. 2004). Other studies have considered impacts of altered Indian Ocean SSTs on Indian monsoon rainfall and on precipitation in eastern central and southern Africa

(e.g., Goddard and Graham 1999; Meehl and Arblaster 2002).

With respect to impacts the winter Northern Hemisphere circulation, Rodwell et al. (1999) showed that an atmospheric general circulation model (AGCM) driven with observed global SSTs and sea ice changes over the latter half of the twentieth century reproduced much of the observed low frequency variability in the NAO. Hoerling et al. (2001) obtained a similar result using only tropical SSTs, indicating the circulation trends reflected the impact of progressive tropical warming. Following this evidence, Bader and Latif (2003) prescribed observed SST variability isolated to individual tropical ocean regions in an AGCM,
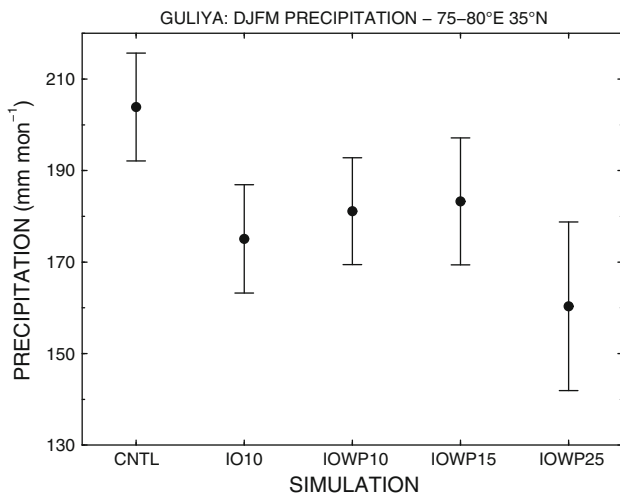
Fig. 16 As in Fig. 10, but for December–March precipitation (mm mon^{-1}) from the region of central Asia near Guliya Ice Cap (75–80°W along 35°N)
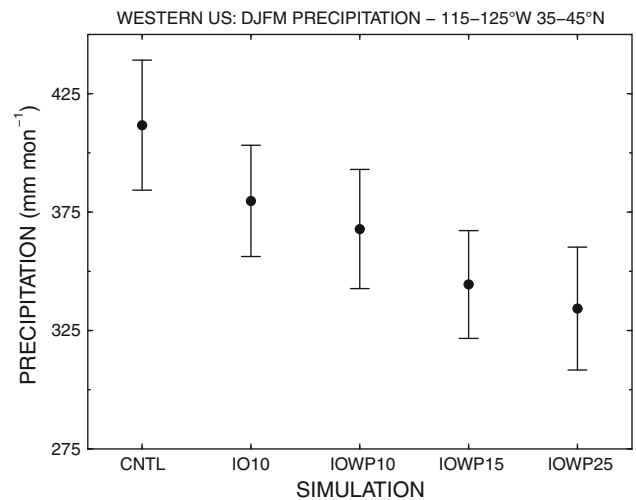

Fig. 18 As in Fig. 10, but for December–March precipitation from the western USA (mm mon^{-1}; 35–45°N, 115°W–125°W)
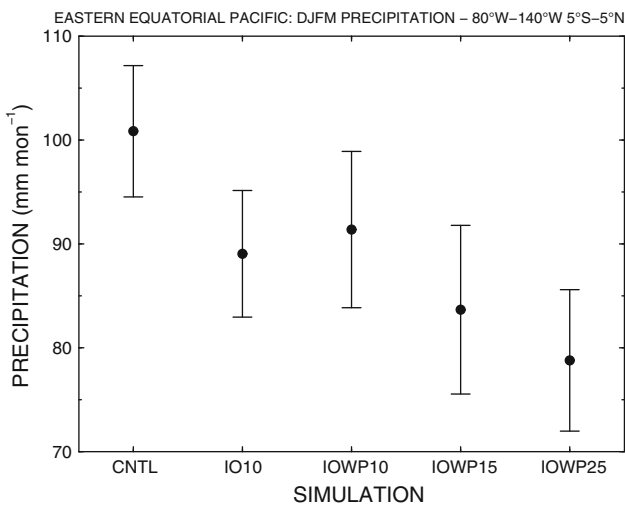
Fig. 17 As in Fig. 10, but for December–March precipitation (mm mon^{-1}) from the eastern equatorial Pacific (5°S–5°N, 80°W–140°W)

concluding that Indian Ocean warming was the dominant driver of the NAO trend. Hurrell et al. (2004) compared the response of several AGCMs to observed SST variability prescribed (i) globally, (ii) only in the tropical oceans, and (iii) only in the tropical Atlantic. Their results were similar to those described above; again implicating changes in tropical ocean SST patterns (and especially Indian Ocean warming) as the cause of the strengthening NAO. These trends were not reproduced in the simulations with an AGCM (CCM3) using only tropical Atlantic SSTs [similar results in this regard were obtained by Pohlmann and Latif (2005) with a different AGCM]. In a companion study, Hoerling et al. (2004) examined AGCM sensitivity to global tropical, Indian-West Pacific and Indian Ocean-only

SST variability. The results with each of these prescribed SST experiments reproduced observed circulation trends, further supporting the findings of Rodwell et al. (1999) and Bader and Latif (2003), and the link between Indian Ocean warming and the a more positive NAO. Bader and Latif (2005) performed experiments much like ours, using a full physics CGCM with prescribed warmer (and cooler) SSTs in the uppermost layer of the Indian Ocean. In their results, the simulated winter NAO closely tracks prescribed Indian Ocean SST changes at decadal and longer time scales. Deser and Phillips (2006) examine the sensitivity of two AGCMs with quite different convective parameterizations to observed late twentieth century global tropical SST changes (a period when both the tropical Indian and Pacific Oceans warmed). Their results emphasize that the magnitude of the changes in convection over the Indian Ocean, and resulting atmospheric response over the North Pacific are sensitive not only to the tropical SST patterns, but to the particular model and parameterizations used as well.

The dynamical processes through which Indian Ocean SSTs elicit robust teleconnections in the winter NH circulation (including the NAO) have also been explored in several studies (Branstator 2000; Hoerling et al. 2004; Lu et al. 2004; Bader and Latif 2005). The results show that disturbances to the NH jet stream over southern Asia that can efficiently propagate over great distances and tend to amplify over the North Atlantic. Changes in deep convection over the Indian Ocean resulting from altered SSTs produce such perturbations, thus providing the dynamical link between Indian Ocean SSTs and the NAO (Hoerling et al. 2004; Bader and Latif 2005).

Addressing the question of the late twentieth century downward trend in Sahel rainfall, Giannini et al. (2003),

Bader and Latif (2003), and Lu and Delworth (2005) describe various AGCM experiments using observed and idealized SSTs prescribed globally or regionally for the tropical oceans. Their results uniformly show that warmer Indian Ocean SSTs result in decreased Sahel precipitation, with the Sahelian anomalies extending east into the Ethiopian Highlands in the latter two studies, as in our results [see Fig. 8 and related text; Giannini et al. (2003) do not show results for eastern Africa]. This latter finding is consistent with the close agreement between low frequency variability in Sahel precipitation during the latter part of the twentieth century and declining trends in Blue Nile and River Atbara discharge, both of which drain the Ethiopian Highlands (Sutcliffe and Parks 1999; see Appendix 1). Bader (2005) addresses the dynamical processes through which Indian Ocean SSTs modulate Sahel summer rainfall and finds that subsidence over the Sahel is enhanced and precipitation suppressed as Indian Ocean SSTs and convective precipitation increase. Hoerling et al. (2006) analyzed the response of Sahel rainfall to observed SST variability during the latter half of the twentieth century in ensemble simulations with several AGCMs. Their results show that the multi-model ensemble closely reproduced the observed trends in summer rainfall across much of North Africa, including the Sahel. Other results (also Hoerling et al. 2006) using more limited sets of models suggest that warming in both the tropical Indian and tropical south Atlantic Oceans is required to reproduce the observed pattern of negative trends in Sahelian rainfall across the full breadth of the continent.

Meehl and Arblaster (2002) studied the impacts of Indian Ocean SSTs on the Indian Monsoon with an AGCM. Their results are similar to ours, with a warmer Indian Ocean resulting in reduced summer precipitation throughout the Horn of Africa and into the southern Arabian Peninsula and a more varied response proceeding west through southern Asia. Goddard and Graham (1999) investigated the response of austral summer precipitation in central east and southern Africa to tropical Indian and Pacific Ocean SST variability. They showed that warmer SSTs in the central tropical Indian Ocean (with climatological SSTs elsewhere) tended to increase precipitation in the central east Africa and decrease precipitation in southern Africa. A similar dipole structure has been observed in instrumental data (Nicholson 1986) and emerges from our tropical warming simulations (Fig. 6; also for simulated annual precipitation, not shown), though, as noted earlier, our results show the increases in precipitation more confined to the coastal region, perhaps because of details in model topographic representation or differences in the patterns of Indian Ocean SST changes and/or cooler SSTs in the eastern tropical Pacific.

4 Discussion

4.1 Relating IOWP simulation results to proxy data and reconstructions

Major features of the differences between the IOWP25 and CNTL results for winter (Sect. 3.2.1; Figs. 6 and 7) can be related to patterns of MCA climate change inferred from proxy records (Sect. 3.1). For example, model results are consistent with proxy evidence for drier conditions over the western US (allowing for the spatial bias in model response, Sect. 2.2), northwest Africa, northern Oman, central Asia and the eastern equatorial Pacific (Fig. 2; Fig. 3 S,H,K,M,Q respectively), and increased precipitation over Britain (Fig. 3D,E). This group of proxy-model similarities is associated with the belt of higher SLP across North America and Eurasia, and enhanced westerlies over the North Atlantic (see Sect. 3.2.1). This pattern incorporates a weakened Aleutian low and stronger NAO, features long suggested by others for the MCA on the basis of regional proxy records (e.g., Lamb 1965; LaMarche 1974; Stine 1994; Keigwin 1996; Cobb et al. 2003; Mangini et al. 2005; MacDonald and Case 2005; Graham et al. 2007; Seager et al. 2007a; Trouet et al. 2009). Interestingly, the main aspects of the extra-tropical NH circulation changes can be reproduced by shifting the climatological pattern slightly poleward, and bear some resemblance to those resulting from expansion of the Hadley Cell in greenhouse warming experiments (e.g. Lu et al. 2007, Frierson et al. 2007; Seager et al. 2007b).

The congruence of a stronger NAO, much warmer SSTs and reduced ice extent in the Nordic Seas in the simulation results allows comparison to high latitude North Atlantic proxy records (Fig. 3A–C; also Fig. 5A,B,D). If extrapolated to the proxy data, the model results indicate that the sharp tenth century increase in North Iceland summer SSTs (Figs. 3C, 5D; which was likely apparent in winter as well) marks a persistent reduction in regional North Atlantic and Nordic sea ice cover (Jensen et al. 2004, Fig. 5A; Massé et al. 2008; Figs. 3B, 5B; see also discussion of Fig. 5, Sect. 3.1) resulting from a more positive "NAO-like" circulation regime. The rapid return to a regime of cooler SSTs 350 years later, now accompanied by the appearance of local winter sea ice on the North Iceland shelf would then mark a tendency towards a weaker NAO and the expansion of regional sea ice in the Nordic Seas and high latitude North Atlantic.

Further support for the idea of a stronger NAO during the MCA is provided by agreement between the simulated (NAO-related) warming in the western North Atlantic off the US (Figs. 7, 9) and that seen in marine proxy records from the region (Keigwin 1996, Fig. 3A; Wanamaker et al. 2008). The few proxy records available from the

mid-latitude North Atlantic in the band where the NAO-related cooling would be expected (Figs. 7, 9) are from the coastal eastern Atlantic, and show no indication of sharp MCA-LIA related changes in marine conditions (Eiriksson et al. 2006), a finding consistent with the relatively weak response of SSTs off Europe to NAO variability (compared to the western North Atlantic; e.g. Visbeck et al. 2003; Figs. 7, 9).

An important point of model-proxy correspondence for boreal winter relates to the indications for cooler SSTs and reduced precipitation over the central/eastern equatorial Pacific during the MCA (Cobb et al. 2003; Rein et al. 2004; Conroy et al. 2008a, b). As noted earlier, in the model these changes appear to reflect both direct (Walker Circulation) effects from the Indian/western Pacific warming and indirect amplification by ocean–atmosphere feedbacks in the eastern tropical Pacific (see discussion of Fig. 7). The simulated cooling (up to 0.5°C) is less than the 0.7–0.8°C indicated by proxy records (Cobb et al. 2003; Conroy et al. 2008b, but the wide range of model sensitivities to tropical Pacific ocean–atmosphere coupling (e.g. Neale et al. 2008) and proxy uncertainties renders a quantitative comparison of the magnitude of cooling problematic. In any case, the resulting reductions in eastern Pacific precipitation may have contributed to the simulated extra-tropical circulation shifts, beyond those resulting from the warmer Indo-Pacific SSTs.

The simulated 10–15% reduction in Ethiopian Highlands summer rainfall is in the range of the ~10% reductions in Blue Nile flood discharge during medieval time indicated by documentary and lacustrine records (Hassan 1981; Kondrashov et al. 2005; Hassan 2007; Fig. 3J; see also Halfman et al. 1994; Appendix 1). As noted earlier, the decrease in model precipitation in the Highlands reflects an inhibited northward migration of the ITCZ into the eastern and central Sahel with the warmer Indian Ocean SSTs, suggesting the possibility of reduced precipitation in that region during the MCA, though currently available regional proxy records are not adequate to address this question (Verschuren 2004). With respect to central east Africa, the model results are consistent with Rift Valley lacustrine proxy records indicating regional MCA aridity (Fig. 3I; Verschuren et al. 2000; Verschuren 2004; Russel et al. 2007), showing clear and reproducible reductions in precipitation away from the coastal strip in this region (Fig. 13; see additional discussion in Sect. 3.2.1).

The model results are consistent with lacustrine proxy evidence indicating reduced West African Monsoon rainfall along the Guinea Coast during the MCA (Shanahan et al. 2009; Fig. 5I). As suggested earlier (Sect. 3.2.2), the simulated precipitation declines appear to be a response to subsidence from increased Indian Ocean convection

(similar results appear in other models using increased Indian Ocean SSTs—e.g., Bader and Latif 2003; Hoerling et al. 2006); however, the cause of the actual MCA reductions in this region remains an open question.

The widespread reductions in simulated summer precipitation covering much of the extreme southeast Arabian Peninsula (Fig. 8) appear consistent with the indications for more arid medieval conditions in the proxy record from southern Oman (Fig. 3L). The simulated increase in coastal upwelling (inferred from surface wind stress) along the southern coast of the Arabian Peninsula (see Sect. 3.2.2; Figs. 8, 9) is in qualitative agreement with proxy indications for higher marine productivity in Omani coastal waters during the MCA (Anderson et al. 2002). As discussed earlier, in the model results the enhanced coastal winds and upwelling result from increased subsidence and lower SLP (a "thermal low") along the continental fringes of the Indian Ocean (changes originating from the increased convection over the ocean), rather than from a strengthening of the large-scale South Asian monsoon.

Proceeding eastward, the model results agree with proxy records in showing a tendency towards increased summer precipitation from eastern India into southeastern Asia, and in central China (Fig. 4 and related discussion; also Fig. 8). Once again however, beyond general tendencies, the spatially heterogeneous patterns in the model results and proxy data caution against overly direct point-for-point model-proxy comparisons. The increased austral winter precipitation over Australia apparent in all our simulations (Fig. 8 and related discussion) are in line with evidence that Lake Eyre was permanently filled during parts of the MCA, again consistent with a relatively warmer western and cooler eastern/central tropical Pacific SSTs (Allen 1985).

The lack of boreal summer cooling in the eastern tropical Pacific in the simulation results (Fig. 9) contrasts with indications from sub-annually resolved corals (Cobb et al. 2003). Whether this discrepancy represents a fundamental challenge for the idea of a warmer MCA Indian-Western Pacific Ocean, or reflects flaws in the character of ocean–atmosphere coupling in the model over the eastern tropical Pacific (e.g., Neale et al. 2008), is open to question. In any case, it likely explains why the model results do not reproduce proxy indications for reduced austral winter precipitation in central Chile during the MCA (Jenny et al. 2002; Fig. 3R). The widespread summer aridity over Central America and the Caribbean Sea in the model results is difficult to interpret in the context of regional proxy records which portray a wide range of MCA-LIA precipitation trends. This is particularly so in view of the lack of simulated eastern tropical Pacific cooling in summer and the regional complexity of Caribbean-Central American climate (Hastenrath 1976; Enfield and Alfaro 1999) [for example, the record from coastal Venezuela

indicates a relatively wet MCA (Haug et al. 2001), that from Panama suggests an arid MCA (Lachniet et al. 2004), while the Yucatan records indicate comparatively little difference between MCA and LIA precipitation (Hoddell et al. 1995)].

The model results do not reproduce the medieval summer warming in Europe indicated by proxy records (e.g., Lamb 1965; Holzhauser et al. 2005; Büntgen et al. 2006; see also Goosse et al. 2006), at least not much beyond the global average temperature increase resulting from the artificially induced warmer tropical SSTs (about 0.5°C). The model results do, however, indicate 5–10% less summer rainfall over Britain, consistent with Lamb's (1965) reconstruction for medieval times (see also Proctor et al. 2000; Charman et al. 2006), this in association with a well developed "summer NAO" SLP pattern (Folland et al. 2008; Fig. 8). These precipitation reductions spread eastward into central Europe, as suggested in Fig. 8, but are much more evident as a spatially coherent pattern without the significance test masking.

Together with other experiments (Sect. 3.3), our simulations demonstrate that modest warming of the Indian-Pacific warm pool can elicit a clear response in global circulation, hydroclimatic and broad-scale SST patterns. Further, they provide a plausible dynamically consistent context within which to view the patterns of MCA-LIA climate change inferred from proxy records—including some features not explained by a cooler eastern/central tropical Pacific alone (Graham et al. 2007; Seager et al. 2007a).

4.2 Possible forcing and mechanisms for tropical SST changes

Our work does not address possible mechanisms that could produce centennial time scale variability in Indian–Western Pacific warming, but rather uses the spatial distribution of inferred medieval climate changes as a guide for deducing the underlying SST changes. The idea that important changes in Indian Ocean SST can occur at multi-decadal time scales is demonstrated by the ~ 0.6°C increase experienced during the second half of the twentieth century (e.g. Hurrell et al. 2004). Furthermore, the sensitivity of Indian Ocean SSTs to small changes in surface flux is underscored by the similar degree of warming that generally appears in simulations of the early stages of anthropogenic warming (Alory et al. 2007) when the increases in the direct greenhouse forcing are modest (~ 0.6 W m^{-2}, about ~ 1 W m^{-2} total; Hoerling et al. 2004; Pierce et al. 2006). To provide some comparison, the 10–25 W m^{-2} prescribed irradiance changes used in our experiments represent about 5–10% of the largest terms in the annual tropical Indian Ocean surface heat flux budget

(latent and solar flux ~ 200–240 W m^{-2}; Esbensen and Kushnir 1981).

Although greenhouse warming simulations commonly produce Indian Ocean warming under modest changes in surface fluxes, they do not generally produce a zonally asymmetric response in tropical Indo-Pacific SSTs (Hoerling et al. 2004), as hypothesized for the MCA and LIA. Similarly, full physics climate models driven with estimated changes in volcanic and solar forcing over the past millennium (Ammann et al. 2007; Mann et al. 2009) show little change in the gradient between central/eastern tropical Pacific and Indo-Pacific warm pool SSTs, though these models do yield mean NH temperature records similar to proxy-based reconstructions (Jansen et al. 2007). In contrast, an intermediate complexity coupled model of the tropical Pacific driven with these past fluxes shows a strong zonally asymmetric tropical response quite similar to that indicated by proxy records (a cooler eastern Pacific, warmer western Pacific during the MCA; Mann et al. 2005) through processes that are well understood (Clement et al. 1996), though some physical processes likely to be important for longer time scales are not included in such models. Additionally, at least one full physics model shows a muted asymmetric tropical SST response to realistic solar irradiance changes through a distinct, but related, set of processes (Meehl et al. 2003), though these results are restricted to decadal, rather than centennial, time scales. Another proposed irradiance-related mechanism acts through the effects of solar forcing on stratospheric temperatures and resulting impacts on the tropospheric circulation over the North Atlantic (Shindell et al. 2001; Mann et al. 2009). Simulations with models that include this process show a decrease in the strength of the NAO periods of reduced solar irradiance, consistent with proxy evidence for parts of the LIA, but little change in tropical SSTs (Mann et al. 2009).

Other mechanisms have been proposed in which changes in extra-tropical NH SSTs induce changes in the eastern Pacific-warm pool temperature gradient and/or changes in ENSO variability (Liu et al. 2000; Clement et al. 2000a, b; Sun et al. 2004; Timmermann et al. 2007a, b). Although the model experiments testing these mechanisms have used SST changes much larger than those suggested by proxy records for the MCA, most indicate northward (southward) shifts in the ITCZ, increased (decreased) equatorial trades, and reduced (increased) ENSO activity and/or cooling (warming) in the tropical Pacific in conjunction with NH warming (cooling). All of the mechanisms rely on ocean–atmosphere feedbacks to amplify their expression in the tropical Pacific and generally indicate reductions in ENSO variability when NH summer temperatures are warmer (see also Fig. 5 and related discussion).

5 Summary and conclusions

Results from coupled climate model simulations forced with warmer tropical Indian and western Pacific SSTs have been described and agree well with important features of MCA-LIA climate change inferred from globally distributed climate proxy records. Many of these similarities, particularly those in the extratropical NH during boreal winter, reflect an expansion of the Hadley cell and a northward shift of zonal circulation features during the MCA, a pattern characterized by a contracted Aleutian low, stronger NAO and ridging extending into central Eurasia. These circulation changes, which are similar to those found by others in related experiments (e.g. Hurrell et al. 2004; Hoerling et al. 2004; Bader and Latif 2005), result in regional precipitation, temperature, SST, and sea ice changes much like those suggested by proxy records. Notably, the pattern of tropical SST change responsible for the proxy-model agreement in our results is strikingly similar to MCA-LIA SST differences in a recent proxy-based reconstruction (Mann et al. 2009). We examine evidence from well-supported proxy records indicating abrupt changes in some local climates at the onset and termination of the MCA. While the coherence and rapidity of these changes is remarkable, additional high resolution records and process studies ("forward modeling") are needed to better understand the degree to which these rapid shifts more generally reflect local sensitivities to slow shifts in background conditions, as opposed to significant changes in major elements of the climate system. On a general note, our results portray the tropical SSTs as the principal (if intermediary) driver for large-scale climate change during the MCA; whether realistic changes in extratropical boundary conditions can produce similar agreement with proxy data from around the planet is a hypothesis that should be tested rigorously with respect to the MCA (see Cane 1998; Timmermann et al. 2007b).

Thus, while important aspects of MCA-LIA climate change remain only loosely constrained by proxy records, and models do not yet provide a complete "from first principles" idea of what occurred, or why, it is encouraging that various research avenues are showing some convergence with respect to the (i) spatial structure of circumhemispheric MCA circulation changes and their associated seasonal imprints on temperature and moisture, (ii) the tropical SST patterns that played a key role in producing the NH circulation changes, and (iii) possible underlying causal mechanisms. It is clear that more work is needed in each of these areas, though it seems that much immediate potential lies with both new quantitative reconstructions of regional precipitation and temperature, most critically for tropical SSTs, and new methods that blend climate model and proxy data (including process studies; e.g., Hughes and Ammann 2009) to provide clearer dynamical perspectives on past climate variability.

Appendix 1: Nile maximum flood level record and derived discharge

The "nilometer" record from Roda Island in Cairo goes back to the seventh century AD and gives the longest records of annual maximum and minimum levels of the Nile (e.g. Sutcliffe and Parks 1999). The record is nearly continuous from 621 to 1469 AD (1 year missing) and after that is patchy through the early 1800s (49% complete) and continuous from 1824 to 1921. Instrumental monthly Nile discharge data are available from Aswan in southern Egypt since 1870 (Vörösmarty et al. 1996), though not useful for this study after 1960, due to abstractions and dam construction. For the results reported here, we use the maximum level record (MAXFL) developed by Kondrashov et al. (2005; Fig. 3J).

Approximately 85% of Nile flood season (August–October) discharge arises from summer precipitation over the central and northern Ethiopian Highlands (drained by the Blue Nile and Atbara, respectively), with the remainder (White Nile) coming in approximately equal parts from a) the southern Ethiopian Highlands and b) farther south in central east Africa and Lake Victoria (Sutcliffe and Parks 1999), the MAXFL record has the potential to provide

information about variability in the extent of the summer northward migration of the ITCZ when it reaches its northernmost position over the Ethiopian Highlands. A difficulty with the "nilometer" records is that siltation has caused the depth of the river bed in Cairo to change over time ("aggradation"; Hassan 1981). Hassan (1981) adjusted the maximum flood level record for changes in recording conventions, converted river level to discharge using modern stage/discharge relationships for Cairo, and tested three different procedures to correct for the effects of aggradation. The results from these methods are quite similar (see Fig. 1A–C in Hassan 1981), and comparison of the record derived using the most conservative of these corrections (Fig. 1C in Hassan 1981) with the MAXFL record indicates that the aggradation bias averages about 1.5 m after 1860 and about 0.9 m for 1688–1859 (a conservatively high estimate), but that the portion of the record including the MCA and early LIA MAXFL levels are not systematically biased high.

We applied the most conservative bias adjustment noted above to the MAXFL record (giving MAXFLADJ) and developed a linear regression between the MAXFLADJ record and measured August-October discharge at Aswan for the period 1870–1921 (the correlation between the Aswan data and the MAXFLADJ record is 0.94). The regression results were then used with the MAXFLADJ record to estimate Nile flood season discharge during the MCA (950–1350) and LIA (1400–1800). The results give average Aswan flood season discharge during the MCA as 38.1 km^3, compared with 42.7 km^3 during the LIA, indicating that average flood season discharge during the MCA was around 11% less than during the LIA (without bias adjustment, the corresponding figure is 20%).

Discharge from the Ethiopian Plateau trended downward between the mid-1950's and about 1985, with Blue Nile annual flow decreasing by about 30% (measured at Roseires Dam, above most modern abstractions) and at least that much in the River Atbara draining the northern Ethiopian Highlands (Sutcliffe and Parks 1999). These trends parallel the decreasing trends in Sahel rainfall (e.g. Dai et al. 2004) and increasing trends in Indian Ocean SSTs (Fig. 19). The association between modern Sahel and Ethiopian Highlands rainfall is further emphasized by the low frequency correspondence between the level of Lake Chad (central Sahel) and Aswan flood season discharge, particularly with both showing substantial declines during the late nineteenth century (not shown; see also Hassan 1981).

Model simulations indicate that Indian Ocean warming was a principal cause of declining Sahelian precipitation during the latter half of the twentieth century (see Sect. 3.4).
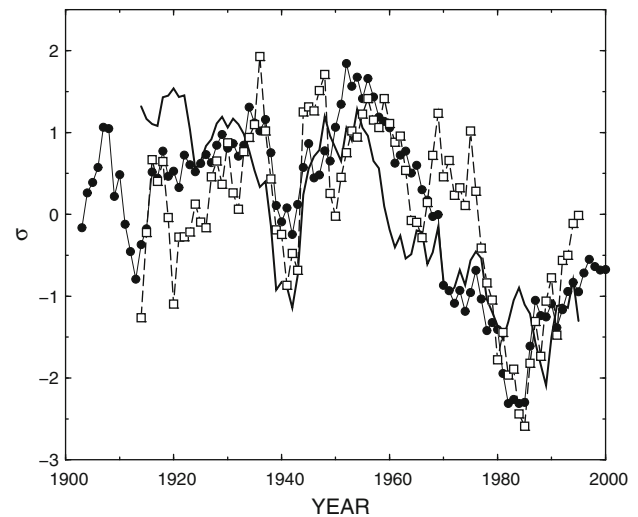

Fig. 19 August–October western Indian Ocean SSTs (*inverted*; average over 10°S–15°N, 40°E–80°E; heavy solid line), western Sahel July–September precipitation (10–20°N, 20°W–10°E; *thin solid line with filled circles*), and peak monthly average Blue Nile discharge at Roseires Dam (*dashed line with open squares*). SST data are from Smith and Reynolds (2004); Sahel precipitation data available from http://jisao.washington.edu/data/sahel; Blue Nile discharge data from Sutcliffe and Parks (1999); all data are normalized 5-year running means. The lowest Blue Nile discharge values are about 25% below the pre-1950s average. Indian Ocean SSTs increased by ∼0.6–0.7°C from the 1950s to the 1980s

References

Agnihotri R, Dutta K (2003) Centennial scale variations in monsoonal rainfall (Indian, east equatorial and Chinese monsoons): manifestations of solar variability. Curr Sci India 85:459–463

Agnihotri RK, Dutta K, Bhushan R, Somayajulu BLK (2002) Evidence for solar forcing on the Indian monsoon during the last millennium. Earth Planet Sci Lett 198:521–527

Alexander MA, Blade I, Newman M, Lanzante JR, Lau N-C, Scott JD (2002) The atmospheric bridge: the influence of ENSO teleconnections on air-sea interaction over the global oceans. J Clim 15:2205–2231

Allen RJ (1985) The Australasian summer monsoon, teleconnections, and flooding in the Lake Eyre Basin. Royal Geographical Society of Australasia, South Australian Geographical Review Papers, vol 2, 47 pp

Alory G, Wijffels S, Meyers G (2007) Observed temperature trends in the Indian Ocean over 1960–1999 and associated mechanisms. Geophys Res Lett 34:L02606. doi:10.1029/2006GL028044

Ammann CM, Joos F, Schimel D, Otto-Bliesner BL, Tomas R (2007) Solar influence on climate during the during the Last Millennium. Proc Natl Acad Sci USA 104:3713–3715

Anderson DM, Overpeck JT, Gupta AK (2002) Increase in the Asian Southwest Monsoon during the past four centuries. Science 297:596–599

Anderson RK, Miller GH, Briner JP, Lifton NA, DeVogel SB (2008) A millennial perspective on Arctic warming from ^{14}C in quartz and plants emerging from beneath ice caps. Geophys Res Lett 35:L01502. doi:10.1029/2007GL032057

Bader J (2005) The role of the Tropical Indian Ocean in the global climate. Doctoral dissertation, University of Hamburg

Bader J, Latif M (2003) The impact of decadal-scale Indian Ocean sea surface temperature anomalies on Sahelian rainfall and the North Atlantic Oscillation. Geophys Res Lett 30:2169–2172

Bader J, Latif M (2005) North Atlantic Oscillation response to anomalous Indian Ocean SST in a coupled GCM. J Clim 18:5382–5389

Bellucci A, Gualdi S, Navarra A (2010) The double-ITCZ syndrome in coupled general circulation models: the role of large-scale vertical circulation regimes. J Clim 23:1127–1145

Bjerknes J (1969) Atmospheric teleconnections from the equatorial Pacific. Mon Weather Rev 97:163–172

Bonan GB, Levis S (2006) Evaluating aspects of the community land and atmosphere models (CLM3 and CAM3) using a dynamic global vegetation model. J Clim 19:2290–2301

Boville BA, Gent PR (1998) The NCAR Climate System Model, Version One. J Clim 11:1115–1130

Bradley RS (2000) 1000 years of climate change. Science 288:1353–1354

Bradley RS, Hughes MK, Diaz HF (2003) Climate in Medieval time. Science 302:404–405

Branstator G (2000) Circumglobal teleconnections, the jet stream waveguide, and the North Atlantic Oscillation. J Clim 15:1893–1910

Buckley BM, Anchukaitis KJ, Penny D, Fletcher R, Cook ER, Sano M, Nam LC, Wichienkeeo A, Minh TT, Hong TM (2010) Climate as a contributing factor in the demise of Angkor, Cambodia. Proc Natl Acad Sci USA 107:6748–6752

Büntgen U, Frank D, Nievergelt D, Esper J (2006) Summer temperature variations in the European Alps, A.D. 755–2004. J Clim 19:5606–5623

Cadet D, Nnoli N (1987) Water vapor transport over Africa and the Atlantic ocean during summer 1979. Q J Roy Meteorol Soc 113:581–602

Cane MA (1998) Climate change: a role for the tropical Pacific in climate change. Science 282:59–61

Cayan DR (1992) Latent and sensible heat flux anomalies over the northern oceans: driving the sea surface temperature. J Phys Oceanogr 22:859–881

Charman DJ, Blundell A, Chiverrell RC, Hendon D, Langdon PG (2006) Compilation of non-annually resolved Holocene proxy climate records: Stacked Holocene peatland palaeo-water table reconstructions from northern Britain. Quat Sci Rev 25:336–350

Clement AC, Seager R, Cane MA, Zebiak SE (1996) An ocean dynamical thermostat. J Clim 9:2190–2196

Clement AC, Seager R, Cane MA (2000a) Orbital controls on tropical climate. Paleoceanography 14:441–446

Clement AC, Seager R, Cane MA (2000b) Suppression of El Niño during the mid-Holocene by changes in the Earth's orbit. Paleoceanography 15:731–737

Cobb KM, Charles CD, Cheng H, Edwards RL (2003) El Niño/Southern Oscillation and tropical Pacific climate during the last millennium. Nature 424:271–276

Collins WD, Rasch PJ, Boville BA, Hack JJ, McCaa JR, Williamson DL, Briegleb PB, Bitz CM, Lin S-J, Zhang M (2006) The formulation and atmospheric simulation of the Community Atmosphere Model: CAM3. J Clim 19:2144–2161

Conroy JL, Overpeck JT, Cole JE, Shanahan TM, Steinitz-Kannan M (2008a) Holocene changes in eastern tropical Pacific climate inferred from a Galápagos lake sediment record. Quat Sci Rev 27:1166–1180

Conroy JL, Restrepo A, Overpeck JT, Steinitz-Kannan M, Cole JE, Bush MB, Colinvaux PA (2008b) Unprecedented recent warming of surface temperatures in the eastern tropical Pacific Ocean. Nature 2:46–50. doi:10.1038/ngeo390

Cook ER, Woodhouse C, Eakin CM, Meko DM, Stahle DW (2004) Long-term aridity changes in the western United States. Science 306:1015–1018

Crowley TJ (2000) Causes of climate change over the past 1000 years. Science 298:270–277

Dai A, Lamb PJ, Trenberth KE, Hulme M, Jones PD, Xie P (2004) The recent Sahel drought is real. Int J Climatol 24:1323–13331

Delworth TL, Greatbatch RJ (2000) Multidecadal thermohaline circulation variability driven by atmospheric surface flux forcing. J Clim 13:1481–1495

Deser C, Phillips AS (2006) Simulation of the 1976/77 climate transition over the North Pacific: sensitivity to tropical forcing. J Clim 19:6170–6180

Deser C, Walsh JE, Timlin M (2000) Arctic sea ice variability in the context of recent atmospheric circulation trends. J Clim 13:617–633

DeWeaver E, Bitz CM (2006) Atmospheric circulation and Arctic sea ice in CCSM3 at medium and high resolution. J Clim 19:2415–2436

Dickinson RE, Oleson KW, Bonan G, Hoffman F, Thornton P, Vertenstein M, Yang Z-L, Zeng X (2006) The community land model and its climate statistics as a component of the community climate system model. J Clim 19:2302–2324

Eiríksson J, Bartels-Jónsdóttir H, Cage A, Gudmundsdóttir E, Klitgaard-Kristensen D, Marret F, Rodrigues T, Abrantes F, Austin W, Jiang H, Knudsen K, Sejrup H (2006) Variability of the North Atlantic Current during the last 2000 years based on shelf bottom water and sea surface temperatures along an open ocean/shallow marine transect in western Europe. Holocene 16:1017–1029

Enfield DB, Alfaro EJ (1999) The dependence of Caribbean rainfall on the interaction of the tropical Atlantic and Pacific oceans. J Clim 12:2093–2103

Esbensen SK, Kushnir Y (1981) The heat budget of the global ocean: an Atlas based on estimates from surface marine observations. Report no. 29, Climatic Research Institute, Oregon State University, 244 pp

Esper J, Frank DC, Büntgen U, Verstege A, Luterbacher J, Xoplaki E (2007) Long-term drought severity variations in Morocco. Geophys Res Lett 34. doi:10.1029/2007GL030844

Fleitmann D, Burns S, Mudelsee M, Neff U, Kramers J, Mangini A, Matter A (2003) Holocene forcing of the Indian Monsoon recorded in a Stalagmite from Southern Oman. Science 13:1737–1739. doi:10.1126/science.1083130

Folland CK et al (1992) In: Houghton JT, Callander BA, Varney SK (eds) Climate change 1992: the supplementary report to the IPCC Scientific Assessment. Cambridge University Press, Cambridge, pp 135–170

Folland CK, Knight J, Linderholm H, Fereday D, Ineson S, Hurrell J (2008) The summer North Atlantic Oscillation. J Clim 22:1082–1103

Frierson DMW, Lu J, Chen G (2007) Width of the Hadley cell in simple and comprehensive General Circulation Models. Geophys Res Lett. doi:10.1029/2007GL031115

Gent PR, Bryan O, Danabasoglu G, Lindsay K, Tsumune D, Hecht MW, Doney SC (2006) Ocean Chlorofluorocarbon and heat uptake during the twentieth century in the CCSM3. J Clim 19:2366–2381

Giannini A, Saravanan R, Chang P (2003) Oceanic forcing of Sahel rainfall on interannual to interdecadal timescales. Science 302:1027–1030

Gill RB (2000) The Great Maya droughts: water, life, and death. University of New Mexico Press, Albuquerque. ISBN:0-826-32194

Goddard L, Graham NE (1999) Importance of the Indian Ocean for simulating rainfall anomalies over eastern and southern Africa. J Geophys Res 104:19099–19116

Goosse H, Arzel O, Luterbacher J, Mann ME, Renssen H, Riedwyl N, Timmermann A, Xoplaki E, Wanner H (2006) The origin of the "European Medieval Warm Period". Clim Past 2:99–113

Graham NE, Hughes MK (2007) Reconstructing the medieval Mono Lake low stands. Holocene 17:1197–1210

Graham NE, Barnett TP, Schlesse U, Bengtsson L (1993) On the role of tropical and mid-latitude SSTs in forcing interannual to interdecadal variability in the winter Northern Hemisphere circulation. J Clim 7:141–1441

Graham NE, Hughes MK, Ammann CM, Cobb KM, Hoerling MP, Kennett DJ, Kennett JP, Rein B, Stott L, Wigand PE, Xu T (2007) Tropical Pacific mid-latitude teleconnections in medieval times. Clim Change 83:241–285

Gray ST, Graumlich LJ, Betancourt JL, Pederson GT (2004) A tree-ring based reconstruction of the Atlantic multidecadal oscillation since 1567 A.D. Geophys Res Lett 31:L12205. doi:10.1029/2004GL019932

Grove JM (1988) The Little Ice Age. Methuen, London

Guilyardi E, Wittenberg A, Fedorov A, Collins C, Capotondi A, van Oldenborgh GJ, Stockdale T (2009) Understanding El Niño in ocean-atmosphere general circulation models: progress and challenges. Bull Am Meteorol Soc 90:325–340

Halfman JD, Johnson TC, Finney BP (1994) New AMS dates, stratigraphic correlations and decadal climatic cycles for the past 4 ka at Lake Turkana, Kenya. Palaeogeogr Palaeocl 111:83–98

Hassan FA (1981) Historical Nile floods and their implications for climatic change. Science 212:1142–1144

Hassan FA (2007) Extreme Nile floods and famines in Medieval Egypt (AD 930–1500) and their climatic implications. Quat Int 173–174:101–112

Hastenrath S (1976) Variations in low-latitude circulation and extreme climatic events in the tropical Americas. J Atmos Sci 33:202–215

Haug GH, Hughen KA, Sigman DM, Peterson LC, Röhl U (2001) Southward migration of the Intertropical Convergence Zone through the Holocene. Science 293:1304–1308

Haug GH, Günther D, Peterson LC, Sigmon DM, Hughen KA, Aeschlimann B (2003) Climate and the collapse of the Maya civilization. Science 299:1731–1735

Hegerl TC, Crowley TJ, Hyde WT, Frame DJ (2006) Climate sensitivity constrained by temperature reconstructions over the past seven centuries. Nature 440:1029–1032

Hoddell DA, Curtis JH, Brenner M (1995) A possible role of climate in the collapse of the classic Maya civilization. Nature 375:391–394

Hoerling MP, Hurrell JW, Xu T (2001) Tropical origins for recent North Atlantic climate change. Science 292:90–92

Hoerling MP, Hurrell JW, Xu T, Bates GT, Phillips AS (2004) Twentieth century North Atlantic climate change. Part II: understanding the effect of Indian Ocean warming. Clim Dyn 23:391–405

Hoerling MP, Hurrell JW, Eischeid J, Phillips A (2006) Detection and attribution of twentieth century northern and southern African rainfall change. J Clim 19:3989–4008

Hoffmann G (2003) Taking the pulse of the tropical water cycle. Science 301:776–777

Holland MM, Bitz CM, Hunke EC, Lipscomb WH, Schramm JL (2006a) Influence of the sea ice thickness distribution on polar climate in CCSM3. J Clim 19:2398–2414

Holland MM, Bitz CM, Tremblay B (2006b) Future abrupt transitions in the summer Arctic sea ice. Geophys Res Lett 33:L32503. doi:10.1029/2006GL028024

Holzhauser H, Magny M, Zumbühl HJ (2005) Glacier and lake-level variations in west-central Europe over the last 3500 years. Holocene 15:789–801

Hughes MK, Ammann CM (2009) The future of the past—an earth system framework for high resolution paleoclimatology: editorial essay. Clim Change 94:247–249. doi:10.1007/s10584-009-9588-0

Hughes MK, Diaz HF (1994) Was there a "Medieval Warm Period" and if so, where and when? Clim Change 26:109–142

Hughes MK, Funkhouser G (1998) Extremes of moisture availability reconstructed from tree-rings from recent millennia. In: Beniston M, Innes JL (eds) Great Basin of Western North America, impacts of climate variability on forests. Springer, Berlin, pp 99–107

Hulme M (1992) Rainfall changes in Africa—1931–1960 to 1961–1990. Int J Climatol 12:685–699

Hurrell JW (1995) Decadal trends in the North Atlantic Oscillation: regional temperatures and precipitation. Science 269:676–679

Hurrell JW, van Loon H (1997) Decadal variations in climate associated with the North Atlantic oscillation. Clim Change 36:301–326

Hurrell JW, Hoerling MP, Phillips AS, Xu T (2004) Twentieth century North Atlantic climate change. Part I: assessing determinism. Clim Dyn 23:371–389

Hurrell JW, Hack JJ, Phillips AS, Caron J, Yin J (2006) The dynamical simulation of the community atmosphere model version 3 (CAM3). J Clim 19:2162–2183

Janicot S, Harzallah A, Fontaine B, Moron V (1998) West African monsoon dynamics and Eastern Equatorial Atlantic and Pacific SST anomalies (1970–1988). J Clim 11:1874–1882

Jansen E, Overpeck J, Briffa KR, Duplessy J-C, Joos F, Masson-Delmotte V, Olago D, Otto-Bliesner B, Peltier WR, Rahmstorf S, Ramesh R, Raynaud D, Rind D, Solomina O, Villalba R, Zhang D (2007) Palaeoclimate. In: Solomon S, Qin D, Manning M, Chen Z, Marquis M, Averyt KB, Tignor M, Miller HL (eds) Climate change 2007: the physical science basis. Contribution of Working Group I to the fourth assessment report of the Intergovernmental Panel on Climate Change. Cambridge University Press, pp 433–497

Jenny B, Valero-Gracés BL, Urrutia R, Kelts K, Veit H, Appleby P, Geyh M (2002) Moisture changes and fluctuations of the Westerlies in Mediterranean Central Chile during the last 2000 years: the Laguna Aculeo record (33°50'S). Quat Int 87:3–18

Jensen K, Kuijpers A, Koç N, Heinemeier J (2004) Diatom evidence of hydrographic changes and ice conditions in Igaliku Fjord, South Greenland. Holocene 14:152–164

Jiang H, Eiriksson J, Schultz M, Knudsen KL, Seidenkrantz MS (2005) Evidence for solar forcing of sea surface temperature on the North Icelandic Shelf during the late Holocene. Geology 33:73–76

Jones TL, Schwaitalla A (2008) Archeological perspectives on the effects of Medieval drought in California. Quat Int 188:41–58

Kaufman DS, Schneider DP, McKay NP, Ammann CM, Bradley RS, Briffa KR, Miller GH, Otto-Bliesner BL, Overpeck JT, Vinther BM (2009) Recent warming reverses long-term Arctic cooling. Science 325:1236–1239

Keigwin LD (1996) The Little Ice Age and Medieval warm period in the Sargasso Sea. Science 274:1504–1508

Kennett DJ, Kennett JP (2000) Competitive and cooperative responses to climatic instability in coastal southern California. Am Antiq 65:379–395

Kiehl JT, Shields CA, Hack JJ, Collins WD (2006) The climate sensitivity of the Community Climate System Model. J Clim 19:2584–2596

Kondrashov D, Feliks Y, Ghil M (2005) Oscillatory modes of extended Nile River records (A.D. 622–1922). Geophys Res Lett 32:L10702. doi:10.1029/2004GL022156

Kushnir Y (1994) Interdecadal variations in North-Atlantic sea-surface temperature and associated atmospheric conditions. J Clim 7:141–157

Kushnir Y, Robinson W, Bladé I, Hall N, Peng S, Sutton R (2002) Atmospheric GCM response to extratropical SST anomalies: synthesis and evaluation. J Clim 15:2233–2256

Lachniet MS, Burns SJ, Piperno D, Asmerom Y, Polyak VJ, Moy CM, Christenson K (2004) A 1500-year El Niño-Southern Oscillation history for the Isthmus of Panama from speleothem calcite. J Geophys Res 109. doi:10.1029/2004JD004694

LaMarche VC (1974) Paleoclimate inferences from long tree-ring records. Science 183:1043–1048

Lamb HH (1965) The early medieval warm epoch and its sequel. Palaeogeogr Palaeocl 1:13–37

Lamb HH (1969) Climatic fluctuations. In: Flohn H, Landsberg HE (eds) World survey of climatology, chap 5, vol 2. Elsevier, New York, pp 173–249

Lamb PJ (1983) West African water vapor variations between recent contrasting Subsaharan rainy seasons. Tellus A 35(3):198

Lau N-C (1985) Modeling the seasonal dependence of the atmospheric response to observed El Niños in 1962–76. Mon Weather Rev 113:1970–1996

Li H, Dai A, Zhou T, Lu J (2008) Response of East Asian summer monsoon to historical SST and atmospheric forcing during 1950–2000. Clim Dyn. doi:10.1007/s00382-008-0482-7

Liu Z, Kutzbach J, Wu L (2000) Modeling climate shift of El Nino variability in the Holocene. Geophys Res Lett 27:2265–2270

Lu J, Delworth T (2005) Oceanic forcing of the late 20th century Sahel drought. Geophys Res Lett 32:L22706.1–L22706.5

Lu J, Greatbatch RJ, Peterson KA (2004) Trend in Northern hemisphere winter atmospheric circulation during the Last Half of the twentieth century. J Clim 17:3745–3760

Lu J, Vecchi GA, Reichler R (2007) Expansion of the Hadley cell under global warming. Geophys Res Lett 34:L06805. doi:10.1029/2006GL028443

Lund DC, Lynch-Stieglitz J, Curry WB (2006) Gulf Stream density structure and transport during the past millennium. Nature 444:601–604. doi:10.1038/nature05277

Luterbacher JD, Dietrich E, Xoplaki E, Grosjean M, Warner H (2004) European seasonal and annual temperature variability, trends and extremes since1500. Science 303:1499–1503

MacDonald G, Case R (2005) Variations in the Pacific decadal oscillation over the past millennium. Geophys Res Lett 32:L08703. doi:10.1029/2005GL022478

Mangini A, Spötl C, Verdes P (2005) Reconstruction of temperature in the Central Alps during the past 2000 yr from a d18O stalagmite record. Earth Planet Sci Lett 235:741–751. doi:10.1016/j.epsl.2005.05.010

Mann ME, Cane MA, Zebiak SE, Clement A (2005) Volcanic and solar forcing of the tropical Pacific over the past 1000 Years. J Clim 18:447–456

Mann ME, Zhang Z, Rutherford S, Bradley RS, Hughes MK, Shindell D, Ammann C, Faluvegi G, Ni F (2009) Global signatures and dynamical origins of the "Little Ice Age" and "Medieval Climate Anomaly". Science 326:1256–1260

Mantua JN, Hare SR, Zhang Y, Wallace JM, Francis RC (1997) A Pacific interdecadal oscillation with impacts on salmon production. Bull Am Meteorol Soc 78:1069–1080

Massé G, Rowland SJ, Sicre M-A, Jacob J, Jansen E, Belt ST (2008) Abrupt climate changes for Iceland during the last millennium: evidence from high resolution sea ice reconstructions. Earth Planet Sci Lett 269:564–568

Meehl GA, Arblaster JM (1998) The Asian-Australian Monsoon and the Southern Oscillation in the NCAR climate system model. J Clim 11:1356–1385

Meehl GA, Arblaster JM (2002) Indian Monsoon GCM sensitivity experiments testing tropospheric biennial oscillation transition conditions. J Clim 15:923–944

Meehl GA, Washington WM, Wigley TM, Arblaster JM, Dai A (2003) Solar and greenhouse gas forcing and climate response in the 20th century. J Clim 16:426–444

Mehringer PJ, Wigand PE (1990) Comparison of Late Holocene environments from woodrat middens and pollen: Diamond Craters, Oregon. In: Betancourt JL, Van Devender TR, Martin PS (eds) Fossil Packrat Middens: the last 40, 000 years of biotic changes. University of Arizona Press, Tucson, pp 294–325

Merryfield WJ, Holland MM, Monahan AH (2008) Multiple equilibria and abrupt transitions in Arctic summer sea ice. In: DeWeaver ET, Bitz CM, Tremblay L-B (eds) Arctic Sea Ice decline: observations, projections, mechanisms, and implications. Geophys Monogr Ser 180. American Geophysical Union, Washington DC, pp 151–174

Moy CM, Seltzer GO, Rodbell DT, Anderson DM (2002) Variability of El Niño/Southern Oscillation activity at millennial timescales during the Holocene epoch. Nature 420:162–165

Mudie PJ, Rochon A, Levac E (2005) Decadal-scale sea ice changes in the Canadian Arctic and their impacts on humans during the past 4, 000 years. Environ Archeol 10:113–126

Muhs DR (1985) Age and paleo-climatic significance of Holocene sand dunes in northeastern Colorado. Ann Assoc Am Geogr 75:566–682

Neale RB, Richter JH, Jochum M (2008) The impact of convection on ENSO: from a delayed oscillator to a series of events. J Clim 21:5904–5924

Newton A, Thunell R, Stott LD (2006) Climate and hydrographic variability in the Pacific warm pool during the last millennium. Geophys Res Lett 33. doi:10.1029/2006GL027234

Nicholson SE (1986) The spatial coherence of African rainfall anomalies: inter-hemispheric teleconnections. J Appl Meteorol Clim 25:1365–1381

Nicholson S (2000) Land surface processes and Sahel climate. Rev Geophys 38:117–139

Nicholson SE, J Kim (1997) The relationship of the El Niño-Southern Oscillation and African rainfall. Int J Climatol 17:117–135

Ogallo LJ (1987) Relationship between seasonal rainfall in east Africa and the southern oscillation. J Climatol 8:31–43

Ogilvie AEJ (1992) Documentary evidence for changes in the climate of Iceland AD 1500 to 1800. In: Bradley RS, Jones PD (eds) Climate since AD 1500. Routledge, London, pp 92–117

Ogilvie AEJ, Jónsson T (2001) "Little ice Age" research: a perspective from Iceland. Clim Change 48:9–52

Opoku-Ankomah Y, Cordery I (1994) Atlantic sea surface temperatures and rainfall variability in Ghana. J Clim 7:551–558

Oppo DW, Rosenthal Y, Linsley BK (2009) 2, 000-year-long temperature and hydrology reconstructions from the Indo-Pacific warm pool. Nature 460:1113–1116

Pfister C, Luterbacher J, Schwarz-Zanetti G, Wegmann M (1998) Winter air temperature variations in western Europe during the Early and High Middle Ages (AD 750–1300). Holocene 8:535–552

Pierce DW, Barnett TP, AchutaRao K, Gleckler P, Gregory J, Washington W (2006) Anthropogenic warming of the oceans: observations and model results. J Clim 19:1873–1900

Pohlmann H, Latif M (2005) Atlantic vs Indo-Pacific influence on European climate. Geophys Res Lett 32:L05707. doi:10.1029/2004GL021316

Proctor C, Baker A, Barnes W, Gilmoor M (2000) A thousand year speleothem proxy record of North Atlantic climate from Scotland. Clim Dyn 16:815–820

Rajagopalan B, Cook E, Lall U, Rey BK (2000) Spatiotemporal variability of ENSO and SST teleconnections to summer drought over the United States during the 20th century. J Clim 13: 4244–4255

Rein B, Lückge A, Sirocko F (2004) A major Holocene ENSO anomaly in the Medieval period. Geophys Res Lett 31:L17211. doi:10.1029/2004GL020161

Richey JN, Poore RZ, Flower BP, Quinn TM (2007) 1400 yr multiproxy record of climate variability from the northern Gulf of Mexico. Geology 35:423–426

Rodwell MJ, Rowell DM, Folland CK (1999) Oceanic forcing of the wintertime North Atlantic Oscillation and European climate. Nature 398:320–323

Ropelewski CF, Halpert MS (1987) Global and regional scale precipitation patterns associated with the El Niño/Southern Oscillation. Mon Weather Rev 115:1606–1626

Russel JM, Verschuren D, Eggermont H (2007) Spatial complexity of 'Little Ice Age' climate in East Africa: sedimentary records from two crater lake basins in western Uganda. Holocene 117:183–193

Schonher T, Nicholson SE (1989) The relationship between California rainfall and ENSO events. J Clim 2:1258–1269

Seager R, Graham N, Herweijer C, Gordon AL, Kushnir Y, Cook E (2007a) Blueprints for Medieval hydroclimate. Quat Sci Rev 26:2322–2336

Seager R, Ting MF, Held IM, Kushnir Y, Lu J, Vecchi G, Huang H-P, Harnik N, Leetmaa A, Lau N-C, Li C, Velez J, Naik N (2007b) Model projections of an imminent transition to a more arid climate in southwestern North America. Science 316:1181–1184

Seager R, Burgman R, Kushnir Y, Clement A, Cook E, Naik N, Miller J (2008) Tropical Pacific forcing of North American Medieval megadroughts: testing the concept with an atmosphere model forced by coral-reconstructed SSTs. J Clim 21:6175–6190

Shanahan TM, Overpeck JT, Sharp WE, Scholz CA, Arko JA (2007) Simulating the response of a closed-basin lake to recent climate changes in tropical West Africa (Lake Botsumtwi, Ghana). Hydrol Process 21:1678–1691

Shanahan TM, Overpeck JT, Anchukaitis KJ, Beck JW, Cole JE, Dettman DL, Peck JA, Scholz CA, King JW (2009) Atlantic forcing of persistent drought in West Africa. Science 324:377–380

Shindell DT, Schmidt G, Mann M, Rind D, Waple A (2001) Solar forcing of regional climate change during the Maunder minimum. Science 294:2149–2152

Sicre M-A, Jacob J, Ezat U, Rousse S, Kissel C, Yiou P, EirIksson J, Knudsen KL, Jansen E, Turon JL (2008a) Decadal variability of sea surface temperatures off North Iceland over the last 2000 years. Earth Planet Sci Lett 268:137–142

Sicre M-A, Yiou P, Eiriksson J, Ezat U, Guimbaut E, Dahhaoui I, Knudsen KL, Jansen E, Turon JL (2008b) A 4500-year reconstruction of sea surface temperature variability at decadal time-scales off North Iceland. Quat Sci Rev 27:2041–2047

Sinha A, Cannariato KG, Stott LD, Cheng H, Edwards RL, Yadava MG, Ramesh R, Singh IB (2007) A 900-year (600 to 1500 A.D.) record of the Indian summer monsoon precipitation from the core monsoon zone of India. Geophys Res Lett 34. doi:10.1029/2007GL030431

Smith TM, Reynolds RW (2004) Extended reconstruction of global sea surface temperature data based on COADS data (1854–1997). J Clim 17:2466–2477

Sokal RR, Rohlf FJ (1969) Introduction to biostatistics. WH Freeman, San Francisco

Stine S (1994) Extreme and persistent drought in California and Patagonia during Medieval time. Nature 369:546–549

Sun D-Z, Zhang T, Shin S-I (2004) The effect of subtropical cooling on the amplitude of ENSO: a numerical study. J Clim 17:3786–3798

Sutcliffe JV, Parks YP (1999) The hydrology of the Nile. International Association of Hydrology, Special Publication no. 5, 180 pp. ISBN:1-901502-75-9

Swetnam TW (1993) Fire history and climate change in Giant Sequoia Groves. Science 262:885–889

Tan L, Cai Y, Yi K, An Z, Ai L (2008) Precipitation variations of Longxi, northeast margin of Tibetan Plateau since AD 960 and their relationship to solar variability. Clim Past 4:19–28

Thompson LG, Mosley-Thompson E, Arnao BM (1984) Major El Niño/Southern Oscillation events recorded in stratigraphy of the tropical Quelccaya Ice Cap. Science 226:50–52

Thompson LG, Mosley-Thompson E, Davis ME, Lin PN, Mikhalenko V, Dai J (1995) A 1000 year ice core climate record from the Guliya Ice Cap, China and its relationship to global climate variability. Ann Glaciol 21:175–181

Timmermann A, Lorenz S, An S-I, Clement A, Xie S-P (2007a) The effect of orbital forcing on the mean climate and variability of the tropical Pacific. J Clim 20:4147–4159

Timmermann A et al (2007b) The influence of a shutdown of the Atlantic meridional overturning circulation on ENSO. J Clim 20:4899–4919

Trouet V, Esper J, Graham NE, Baker A, Frank D, Scourse J (2009) Centuries-long positive North Atlantic Oscillation mode dominated Medieval warm period. Science 324:78–80

Turner BF, Gardner LR, Sharp WE (1996) The hydrology of Lake Bosumtwi, a climate-sensitive lake in Ghana, West Africa. J Hydrol 183:243–261

Verschuren D (2004) Decadal and century-scale climate variability in tropical Africa during the past 2000 Years. In: Battarbee RW, Gasse F, Stickley CE (eds) Conference on climate variability through Europe and Africa. Springer, London, pp 139–158

Verschuren D, Laird K, Cumming B (2000) Rainfall and drought in east Africa during the past 1100 years. Nature 403:410–414

Visbeck M, Chassignet E, Curry R, Delworth T, Dickson R, Krahmann G (2003) The ocean's response to North Atlantic Oscillation variability. In: Hurrell J, Kushnir Y, Ottersen G, Visbeck M (eds) The North Atlantic Oscillation: climatic significance and environmental impact. Geophysical Monograph Series 134. American Geophysical Union, Washington DC, pp 113–145

Vizy EK, Cook KH (2002) Development and application of a mesoscale climate model for the tropics: influence of sea surface temperature anomalies on the West African monsoon. J Geophys Res 107(D3):4023. doi:10.1029/2001JD000686

von Rad U, Schaaf M, Michels KH, Schulz H, Berger WH, Sirocko F (1999) A 5000-yr record of climate change in varved sediments from the oxygen minimum zone off Pakistan, northeastern Arabian Sea. Quat Res 51:39–53

Vörösmarty CJ, Fekete B, Tucker BA (1996) River discharge database, version 1.0 (RivDIS v1.0), vols 0 through 6. A contribution to IHP-V theme 1. Technical Documents in Hydrology Series, UNESCO, Paris

Vuille M, RS Bradley, Werner M, Healy R, Keimig F (2003a) Modeling d^{18}O in precipitation over the tropical Americas: 1. Interannual variability and climatic controls. J Geophys Res 108(D6):4174. doi:10.1029/2001JD002038

Vuille M, Bradley RS, Healy R, Werner M, Hardy DR, Thompson LG, Keimig F (2003b) Modeling d^{18}O in precipitation over the tropical Americas: 2. Simulation of the stable isotope signal in Andean ice cores. J Geophys Res 108(D6):4175. doi:10.1029/2001JD002039

Wanamaker AD, Kreutz KJ, Schöne BR, Pettigrew NR, Borns HW, Introne DS, Belknap D, Maasch KA, Feindel S (2008) Coupled North Atlantic slope water forcing on Gulf of Maine temperatures over the past millennium. Clim Dyn 31. doi:10.1007/s00382-0070344-8

Wang YJ, Cheng H, Edwards RL, He YQ, Kong XG, An ZS, Wu JY, Kelly MJ, Dykosk CA, Li XD (2005) The Holocene Asian monsoon: links to solar changes and North Atlantic climate. Science 308:854–857

Wang N, Jiang X, Thompson L, Davis M (2007) Accumulation rates over the past 500 years recorded in ice cores from the northern and southern Tibetan Plateau, China. Arct Antarct Alp Res 39:671–677

Weldeab S, Lea DW, Schneider RR, Andersen N (2007) 155,000 Years of West African Monsoon and Ocean thermal evolution. Science 316:1303–1307

Woodhouse CA (2004) A paleo-perspective on hydroclimatic variability in the western United States. Aquat Sci 66:346–356

Woodhouse CA, Overpeck JT (1998) 2000 years of drought variability in the central United States. Bull Am Meterol Soc 79:2693–2714

Yang B, Wang J, Bräuning A, Dong Z, Esper J (2009) Late Holocene climatic and environmental changes in arid central Asia. Quat Int 194:68–78. doi:10.1016/j.quaint.2007.11.020

Zhang P et al (2008) A test of climate sun and culture relationships from an 1810-year Chinese cave record. Science 322:940–942

Zheng J, Wang W-C, Ge Q, Man Zm Zhang P (2006) Precipitation variability and extreme events in eastern China during the past 1500 years. Terr Atmos Ocean Sci 17:579–592

Zhou T, Yu R, Zhang J, Drange H, Cassou C, Deser C, Hodson DL, Sanchez-Gomez E, Li J, Keenlyside N (2009) Why the Western Pacific subtropical high has extended westward since the late 1970s. J Clim 22:2199–2315